

Project Thesis

# Design and Evaluation of an EMG-based Recording and Detection System

Clemens Amon

submitted to the  
Institute of Electronic Music and Acoustics  
of the  
University of Music and Performing Arts Graz

in June 2013

**Supervisor:**  
MSc Ph.D. Georgios Marentakis



## Abstract

The project investigates the usability of muscle contractions detected by surface electromyography (EMG) sensors as an input channel for the gestural or subtle control of electric devices. A wearable hardware prototype is presented that consists of a sensor strap and a signal conditioning (amplification and filtering) unit. Signal detection techniques are discussed and an evaluation framework is presented based on signal detection theory. Using the framework common envelope tracking techniques are compared in a user study that uses the prototype. This work forms the basis for further research on using EMG signals for controlling, regulation, and navigation purposes as well as music performance.

### **Zusammenfassung**

Das Projekt untersucht die Nutzbarkeit von Muskelkontraktionen, die durch Elektromyografie-Oberflächensensoren (EMG) abgenommen werden, als Eingangskanal für gestische oder feinsinnige Steuerung von elektronischen Geräten. Ein tragbarer Hardware-Prototyp wird vorgestellt, der aus einem Sensorband und einer Einheit zur Signalaufbereitung (Verstärkung und Filterung) besteht. Techniken der Signalerkennung werden behandelt und eine auf der Signalentdeckungstheorie basierende Evaluierungsumgebung wird präsentiert. In einer Studie werden bekannte Methoden zur Hüllkurvendetektion verglichen und ausgewertet. Diese Arbeit bildet eine Grundlage für weiterführende Untersuchungen im Bereich der Steuerung, Regelung und Navigation durch EMG-Signale, aber auch die Grundlage für die Integration von EMG-Signalen in musikalischen Aufführungen.

## Contents

<b>1</b>	<b>Introduction</b>	<b>1</b>
1.1	Motivation . . . . .	1
1.2	Background . . . . .	1
1.3	Outline . . . . .	2
<b>2</b>	<b>Basic of Electromyography</b>	<b>3</b>
2.1	Physiology . . . . .	3
2.1.1	Myoelectric Signals . . . . .	3
2.1.2	Superposition of the Action Potentials . . . . .	3
2.2	Sensing and Positioning . . . . .	5
2.2.1	The EMG Signal . . . . .	6
2.3	Amplification . . . . .	10
2.4	Noise and interferences affecting EMG signal . . . . .	10
2.5	Signal Processing . . . . .	11
<b>3</b>	<b>Hardware Implementation</b>	<b>13</b>
3.1	Approach in Concept and Design . . . . .	13
3.2	Development and Implementation . . . . .	14
3.2.1	Sensor Unit . . . . .	14
3.2.2	Amplification and Filter Unit (AFU) . . . . .	15
3.3	Reliability, Annoyances - Discussion . . . . .	20
<b>4</b>	<b>Theory in EMG Signal Processing</b>	<b>21</b>
4.1	Notch and band-pass filtering . . . . .	21
4.2	Rectification and Smoothing . . . . .	23
4.3	Signal Detection Theory . . . . .	26
4.3.1	Probability Density Function (PDF) . . . . .	26
4.3.2	Receiver Operating Characteristics . . . . .	28
4.3.3	Double Threshold Detection . . . . .	29

<b>5 Evaluation</b>	<b>32</b>
5.1 User Study . . . . .	32
5.1.1 Test 1 . . . . .	32
5.1.2 Test 2a . . . . .	32
5.1.3 Test 2b . . . . .	32
5.2 Evaluation Results . . . . .	33
<b>6 Conclusion</b>	<b>43</b>
6.1 The live scenario . . . . .	43
6.2 Possible Enhancements . . . . .	44
6.2.1 Hardware . . . . .	44
6.2.2 Software . . . . .	44
<b>A Additional user study recordings</b>	<b>47</b>
<b>B Discrete amplifier test setup</b>	<b>47</b>
<b>C Printed circuit board layout</b>	<b>48</b>
C.1 List of Parts . . . . .	49

# 1 Introduction

## 1.1 Motivation

In the last years gesture interaction between humans and computers became more important. This is because there is an increased need for subtle control systems which makes myoelectric signals interesting. In particular in the field of computer music such signals are valuable as they can be used to augment a musical or dancing performance. In this project, Electromyography (EMG) signals are processed and detected and an interface is designed and evaluated in a control setting.

## 1.2 Background

The idea of using EMG for system control is not new. In 1990 Knapp and Lusted introduced "Biomuse" a bioelectric controller for computer music applications [RBK90]. This system consists of two separate components. A bioelectric interface and a signal processing unit. The bioelectric interface consists of electrodes and sensors that are placed on the user's body, which sense Electromyography (EMG) , Electroencephalography (EEG) i.e. the brain's electrical activity, and EOG (Electrooculography) i.e. eye movement activity. The incoming signals are connected to a patchbox and are then processed in the signal processing unit. There the signals are digital-analog converted, filtered and analysed by a digital signal processing (DSP) chip. The unit analyses all input signals in real-time and receives and sends information to a host computer over a standard RS-232 serial interface. In addition, it receives and sends MIDI information. The Biomuse can be used to control synthesizers, sequencers, drum machines, or any other MIDI device.

Tanaka also used bioelectric signals to realize interaction in the context of music performance [TKA02]. Tanaka describes a system where EMG is combined with relative position sensing to overcome the inability of EMG to measure isotonic movements. EMG measures muscle activity without motion (isometric) very well, but motion without change in tension (isotonic) relatively poorly. Like in the "Biomuse" project, the aim was to create multimodal interaction to increase the number of inputs to the control system and consequently the number of independent parameters that define the interaction.

Costanza, Inverso and Allen proposed in [CIA05] and [CIAM07] another approach of using EMG signals for control purposes. Here, the bioelectrical signals were used to create interfaces that allow subtle and minimal mobile interaction, without disruption of the surrounding environment. Using a wireless EMG device, subjects performed walking tasks while making contractions of different durations. These motionless gestures were sensed and detected online. An action was triggered if the signal exceeded a certain threshold for a predefined time. Costanza et al. showed that EMG can be used successfully as a controller. Using their detection method the contraction needs to be finished in order to be analysed. So time exact triggering is difficult to

realise.

In [NKV<sup>+</sup>] hand gestures were identified by analysing a four-channel EMG with independent component analysis (ICA), where a signal is decomposed in their independent components. This method is used in bio-signal applications to isolate signals from different muscles and analyse them individually. Human hand gestures are used very often in non verbal interactions among people. Thus their interpretation in human computer interaction (HCI) will be a more interesting, especially in cases in which no physically controller (like a computer mouse, or any pointing device) is available or the use of a controller is not wanted.

Advances in integrated circuit technology allow the inclusion of high sensitivity low noise amplifiers in embedded, battery operated, devices at low cost. This enables the construction of small, wearable, intimate devices, that can be used to controlling musical instruments, in the field of rehabilitaion engineering, and in the design of intimate interactions. In nearly all previous works, in which EMG was used, the amplitude envelope of the EMG was extracted via a straightforward RMS calculation. Beyond that more parameters like median frequency can be extracted out of the signal to achieve more degrees of control for the user and to open possibilities for the creation of new sounds and new ways of controlling them.

### 1.3 Outline

This report starts by providing the physiological and technical background on EMG signal acquisition (section 2) and then describes in detail the EMG signal and its acquisition and processing. The development of an EMG hardware device (section 3) is then presented and a software implementation of signal filtering and amplitude extraction is introduced (section 2.5). Two ways of detecting the digital EMG signal and their realisation in MATLAB are presented in sections 4.3 and 4.3.3. In section 5.1 the results of an user study are presented where the introduced methods are tested and analysed and evaluated using signal detection theory (section 5). An application for using this system in a live and real-time environment is designed (section 6.1).

## 2 Basic of Electromyography

### 2.1 Physiology

#### 2.1.1 Myoelectric Signals

Myoelectric signals are measurable signals which appear during muscle activation. During muscle contraction, small electrical currents are generated by the exchange of ions across muscle fiber membranes [Win99, 26]. There are two types of EMG: surface electromyography (SEMG, non-invasive) and needle electromyography (NEMG, invasive). Surface EMG records muscle activity on the skin surface that surrounds a muscle. Electrodes are attached to the skin and provide a crude assessment of the muscle activity below. SEMG provides information on the onset time, duration and relative intensity of muscle activation. While an electrode is placed over the muscle on the skin in SEMG, a needle inserted through the skin into the muscle is used in needle EMG. Needle EMG is more accurate and is therefore preferred in medical diagnostics for the assessment of muscle disease or ongoing pathology [JER]. Invasive needle electrodes acquire signals better and can access individual muscle fibres. In surface EMG the signal is a composite of all the muscle fiber action potentials occurring in the muscles underlying the skin. Intra-muscular recordings can be painful and have only medical applications. Surface electrodes do not inflict pain to the user and for this reason they are preferred in HCI and are used in this project to acquire muscle activity in satisfactory quality, as we will see later. There are two types of SEMG electrodes: wet and dry SEMG electrodes. SEMG electrodes are applied to the skin using conductive gel as an intermediate layer to ensure good conductivity between the skin and the electrode. It is recommended to clean the skin before placing the electrodes using either rubbing alcohol or a special skin preparation fluid for SEMG.

#### 2.1.2 Superposition of the Action Potentials

The nervous system controls muscle contraction by activating discrete motor units and the corresponding muscle fibers at variable firing rates. The number of muscle fibers within each unit can vary. The activation of a motor unit leads to the activation of all its muscle fibers. Muscle tissue conducts electrical potentials similar to the way nerves do. These are called muscle action potentials (MAP). The combination of the muscle fiber action potentials from all the muscle fibers of a single motor unit yields the motor unit action potential (MUAP) [BJ85]. This is the linear sum of all active motor units. Figure 2.1 shows the structure and the produced tension of the motor units and its corresponding muscle fibres.

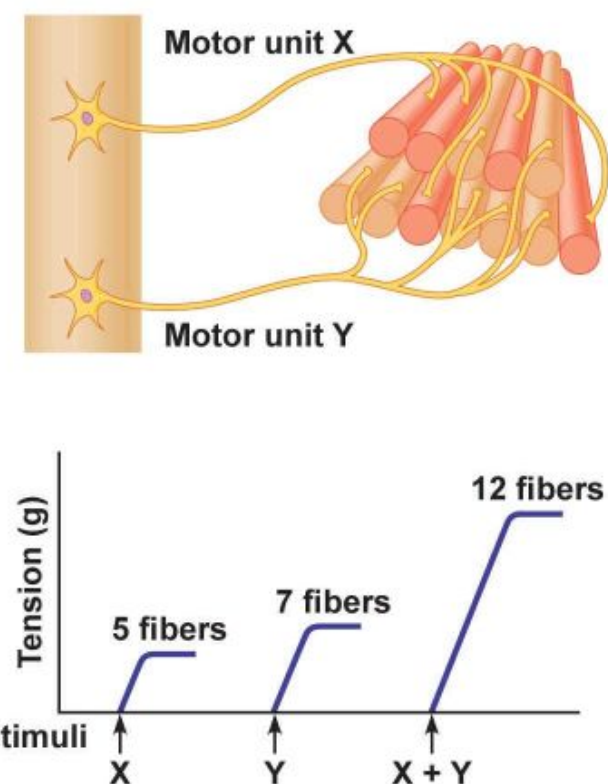


Figure 2.1: Structure of the motor units and the tension when a single or more motor units are activated [Dis11]

## 2.2 Sensing and Positioning

A muscle contraction does not give rise to a single MUAP, but results in MUAP sequences from different motor units, whose superposition is the acquired EMG signal. The amplitude of each single MUAP depends on the distance of the firing motor unit to the electrode and the filter characteristics of the tissue. A higher distance to the electrode leads to a decrease in the amplitude. Figure 2.2 shows a simplified illustration of the superposition of action potentials from different motor units acquired with needle EMG.

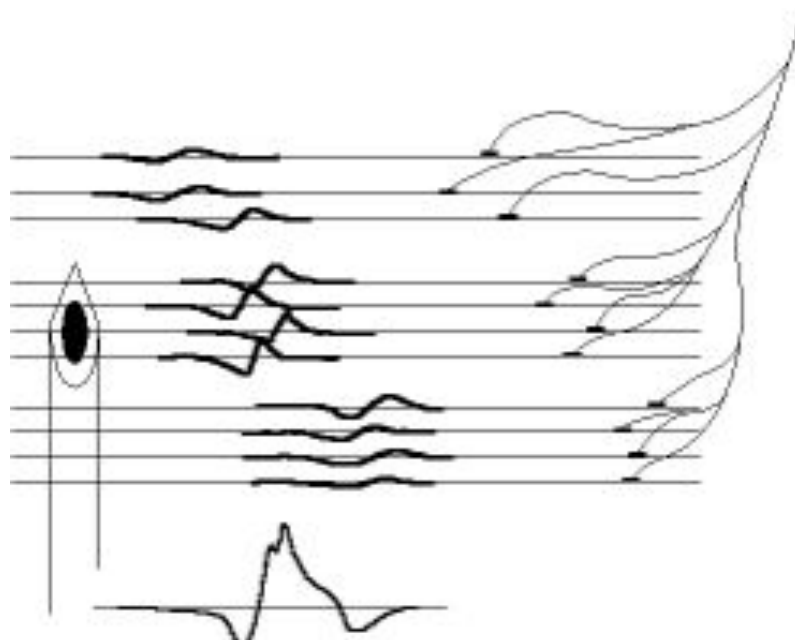


Figure 2.2: Superposition of MUAPs [Kon05, 8]: Three motor units each firing one single MUAP. The first motor unit consists of three muscle fibres and the second and the third motor unit consists of four muscle fibres. The superposition is recorded with a needle electrode. Due to the filter characteristics of the tissue the amplitude of the single impulses of the muscle fibres with a greater distance to the electrode are smaller than the amplitude of the impulses of the muscle fibres close to the electrode.

MUAP sequences are specified by two values: The firing rate  $F_F$ , and the inter-pulse intervals (IPI).  $F_F$  describes the number of discharges over a certain time period, and is measured in Hertz (Hz). More demonstratively the firing rate is usually specified in the SI<sup>1</sup> base unit  $s^{-1}$ . The inter-pulse intervals (IPI)  $T_F$  is a list of periods between successive MUAPs. The instantaneous firing rate is obtained by inverting  $T_F$ . The discharge properties are stochastic. Instead of discharging APs with a constant inter-pulse interval, the timing of successive APs fluctuates. Most

<sup>1</sup> Abbr. for fr.: Le Système international d'unités, International System of Units

studies indicate that the minimum firing or firing rate is between 5 and  $7\text{ s}^{-1}$ . The highest initial rate of discharge varies among studies, but commonly ranges between 12 and  $26\text{ s}^{-1}$  [Win99, 26].

The signal acquisition starts with the recording of the signal at the skin with surface electrodes. Three electrodes are needed to derive the differential EMG signal: Two electrodes which are connected to the 2 inputs of the differential amplifier and a reference electrode which is used to define a ground signal. According to the recommendations of the Surface ElectroMyoGraphy for the Non-Invasive Assessment Project of Muscles (SENIAM), for sensor locations in arm, or hand muscles, but also in hip, or upper leg muscles the two electrodes should be placed in a distance of 20mm. Figure 2.3 is illustrating the SENIAM Recommendations.

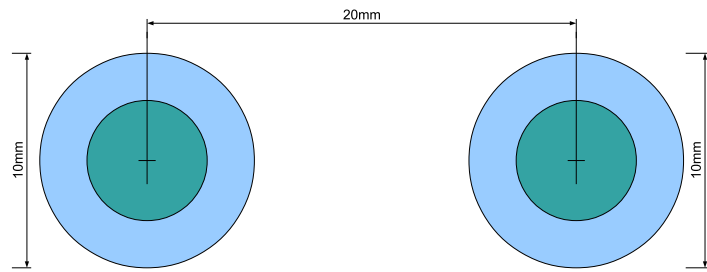


Figure 2.3: Recommendations for sensor locations due to SENIAM

De Luca in [DL97] gives the following recommendations for the location of the electrodes on the measured muscle:

Locate the electrode on the midline of the muscle belly, between the myotendinous junction and the nearest innervation zone, with the detection surface oriented perpendicularly to the length of the muscle fibers. Use electrical stimulation or surface electrical mapping to locate the innervation zones.

### 2.2.1 The EMG Signal

The unfiltered and unprocessed EMG signal is called the raw EMG signal. Equation (2.1) shows a simple model of the EMG signal:

$$x(n) = \sum_{r=0}^{N-1} h(r)e(n-r) + w(n) \quad (2.1)$$

where  $x(n)$  is the modelled EMG signal,  $e(n)$  the point processed firing impulses of the individual motor units ( $r$  represents the time delay of each impulse),  $h(r)$  is the impulse response of the MUAP that is used to combine the individual motor unit impulses,  $w(n)$  is the zero mean

additive white Gaussian noise, and  $N$  is the number of motor unit firings. This model shows the response of the system, here the MUAP, to a series of delayed impulses and is not regarding the filtering characteristics of the tissue.

Figure 2.4 shows a raw EMG Signal of a sequence of dynamic contractions and the noise without muscle activity recorded with BETTERWITTS surface electrodes placed at extensor male. When the muscle is relaxed the noise floor can be seen. The noise depends on many factors that affect signal quality: the amplifier specification and its common mode rejection ratio (CMRR), the quality of the surface electrodes, the way the setup is realized (i.e. the number of electrodes used), and the quality of the cables used (shielded or unshielded) used, and movement artifacts that can occur during recording (i.e. when the cables are not fixed).

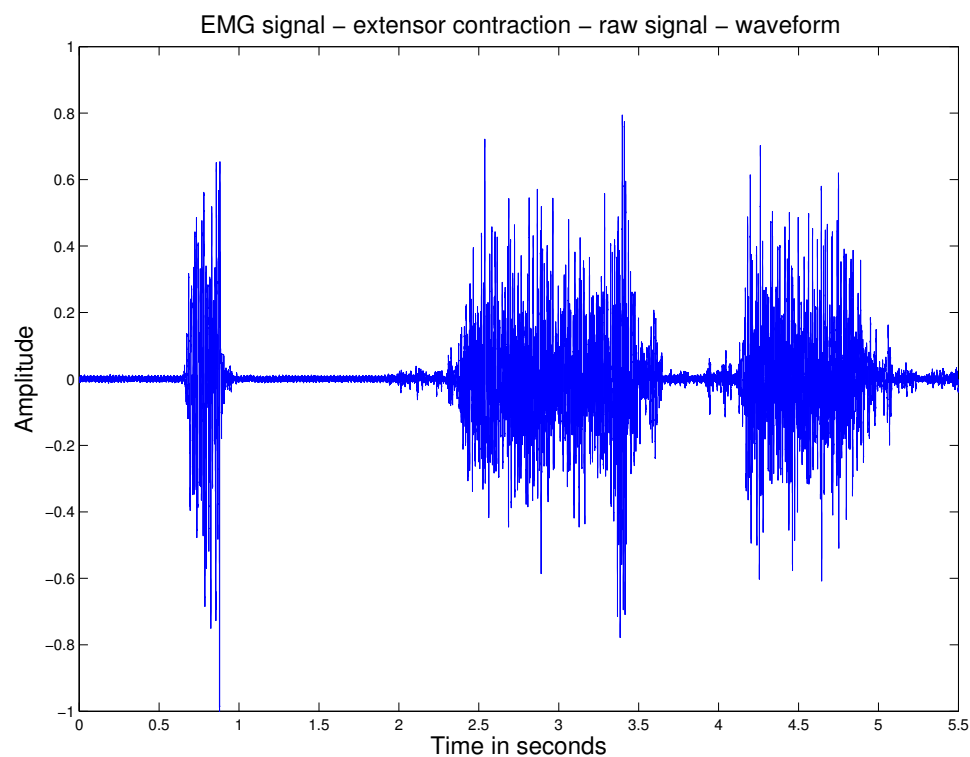


Figure 2.4: EMG Signal and Noise in the time domain

In figure 2.5, the frequency response of the raw EMG signal of a static contraction of extensor male and the frequency response of the noise recorded at extensor male without voluntary muscle activity is shown. A strong 50 Hz power line interference can be seen in the noise figure. Figure 2.6 shows the power spectrum of a short and a long contraction of musculus extensor male with a window size of 200 ms (8820 samples at sample rate of 44.1 kHz). The green and blue ranges mark the signal used for the fft plot. It can be seen that the useful frequency range of the signal extends between 20 Hz and 500 Hz, while most of the energy is distributed from 50 Hz to 400 Hz.

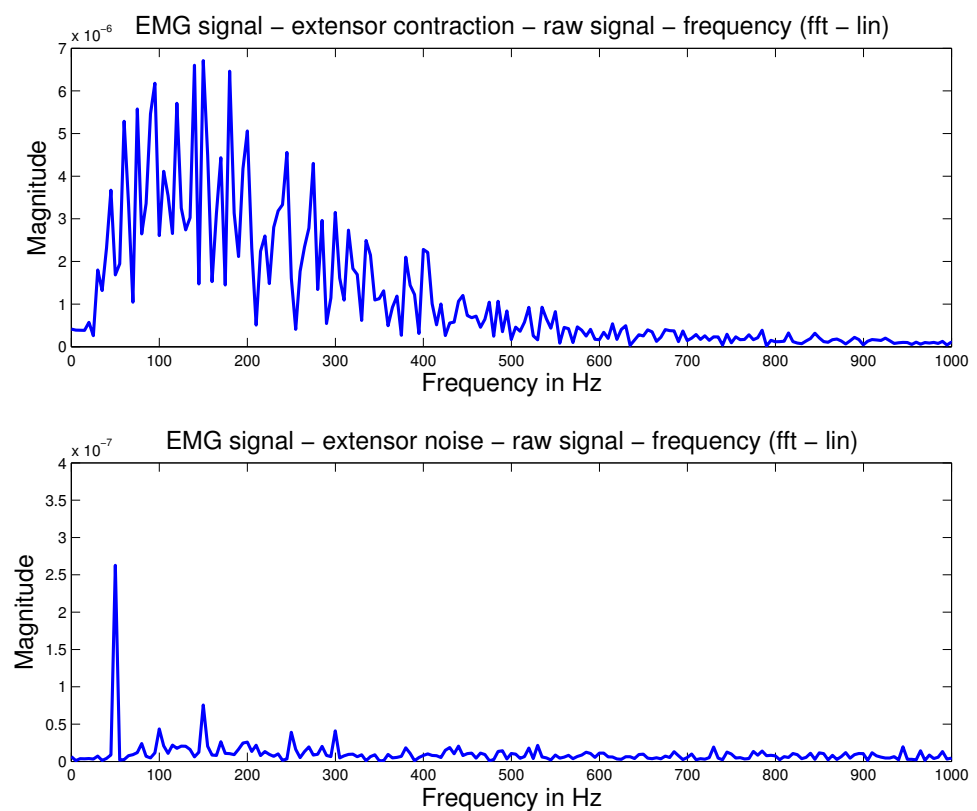


Figure 2.5: EMG Signal and Noise in the frequency domain

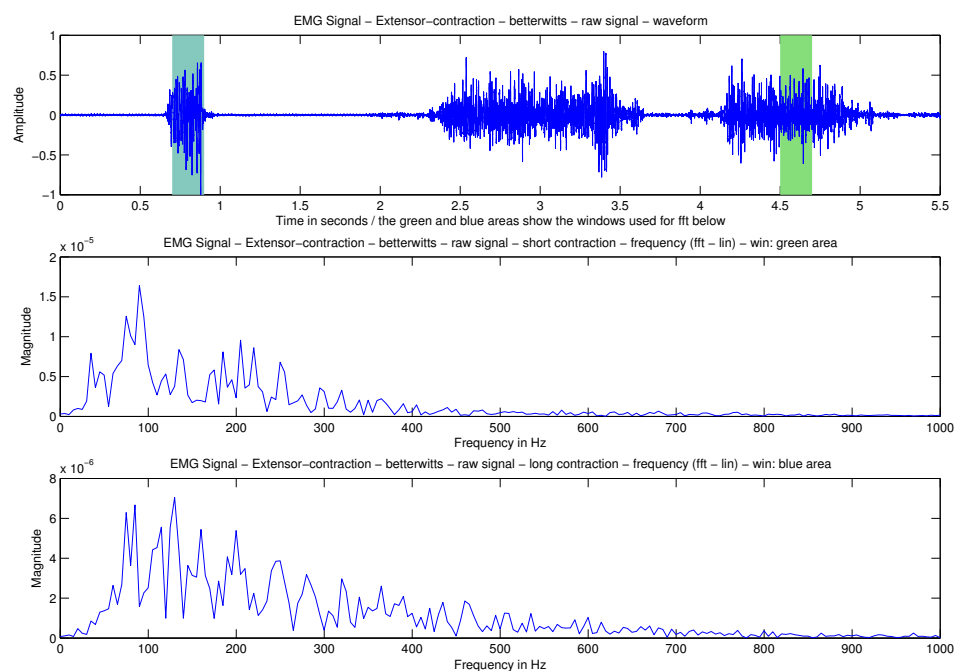


Figure 2.6: (1) raw time signal with fft window marked, (2) power spectrum of a short contraction, (3) power spectrum of a long contraction

## 2.3 Amplification

The amplitude of the superimposed MUAPs is very small (0 to 10 mV) and needs to be amplified. Since the difference of the two electrodes is amplified, it is important that the amplifier has a high Common Mode Rejection Ratio ( $\text{CMRR} > 90\text{dB}$ ). The CMRR describes the accuracy with which a differential amplifier rejects common input, i.e. subtracts one input from the other, relative to the gain with which the difference in its inputs is amplified. The CMRR is measured in Decibel (dB). To achieve the necessary gain factor a multi-stage amplification design is needed. Typically a differential amplifier is used in the first stage [RHMY06]. In the second stage an active inverting operational amplifier is used to get the desired signal amplitude. Before being analog to digital converted and processed, the signal can be filtered to eliminate low-frequency or high-frequency noise, or other possible artifacts. The block diagram of a basic EMG sensor and amplification system is shown in figure 2.7.

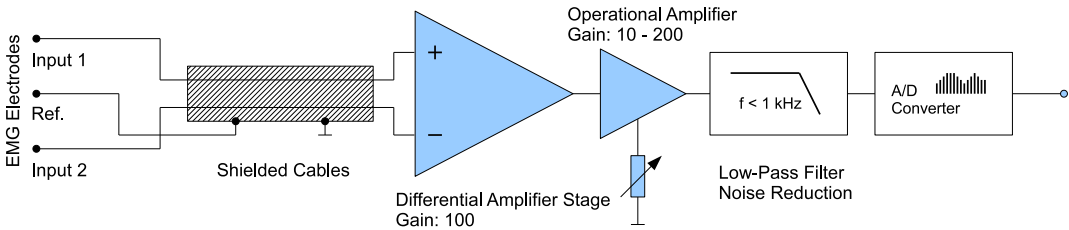


Figure 2.7: Block diagram of an EMG sensor and amplification network

## 2.4 Noise and interferences affecting EMG signal

Two main issues influence the fidelity of the signal. The first is the signal-to-noise ratio (SNR), that is the ratio of the energy in the EMG signals to the energy in the noise signal. In general, noise is defined as electrical signals that are not part of the desired EMG signal. The power line radiation (50 Hz) is a common source of noise in the field of EMG. The second is the distortion of the signal waveform caused by filtering, meaning that the relative contribution of any frequency component in the EMG signal should not be altered to avoid phase shifts [RHMY06]. Therefore the use of analog and digital infinite impulse response (IIR) filters should be minimized, as these filters may introduce frequency-dependent phase shifts in the EMG signal. This can result in increased response onset latency and distortion of the input waveform. If filtering is desired, any detecting and recording device should process the signal linearly. E.g. in [Luc02] De Luca recommends to avoid the implementation of a 50 Hz notch filter when there are alternative methods of dealing with the power line radiation. Symmetrical digital finite impulse response (FIR) filters do not cause phase shifts. In contrast to single user live scenarios, where latency should be avoided, in within-participants designs phase shifts and the accompanying increased latencies are less problematic because they are consistent across experimental conditions. As

the distortion of the signal waveform must be kept low, an analog filter with linear phase shift (a Bessel type filter), which does induce a time shift but produces minimum signal distortion can be applied [BCF<sup>+05</sup>].

Raez et al. [RHMY06] categorizes the electrical noise, which will interfere with the EMG signals into the following types:

1. Inherent noise in electronics equipment: All electronics equipment generate noise. This noise cannot be eliminated; using high quality electronic components can only reduce it.
2. Ambient noise: Electromagnetic radiation is the source of this kind of noise. The surfaces of our bodies are constantly inundated with electric-magnetic radiation and it is virtually impossible to avoid exposure to it on the surface of earth. The ambient noise may have amplitude that is one to three orders of magnitude greater than the EMG signal.
3. Motion artifacts: Motion artifacts cause irregularities in the data. There are two main sources for motion artifacts: 1) electrode interface and 2) electrode cable. Motion artifacts can be reduced by proper design of the electronics circuitry and set-up.
4. Inherent instability of signal: The EMG signal is stochastic in nature. EMG signal is affected by the firing rate of the motor units, which, in most conditions, fire in the frequency region of 0 to 20 Hz. This kind of noise is considered as unwanted and the removal of the noise is important.

## 2.5 Signal Processing

As mentioned before, the useful frequency range is between 0 Hz and 500 Hz. So filtering the raw signal is recommended to limit the signal's frequency range to the desired range. Van Boxtel in [vB08] found that a band-pass frequency range of 20 Hz to 500 Hz appeared to be adequate because there was a negligible contribution of higher frequency components to the EMG signal. In [CJDLR10] De Luca et al. are recommending to set the low-pass filter corner frequency to 400 - 450 Hz, where the high end of the SEMG frequency spectrum is expected. Various recommendations for the high-pass filter corner frequency can be found in literature. All the recommendations are between 5 Hz and 20 Hz. SENIAM recommends to set the high-pass filter corner frequency to 10 - 20Hz.

For several decades it has been commonly accepted that the preferred manner for processing the EMG signal after filtering was to calculate the integrated rectified signal. This was done by full-wave rectifying the EMG signal, integrating the signal over a specified interval of time and subsequently forming a time series of the integrated values. Full-wave rectification means the conversion of the input waveform to one of constant polarity (positive or negative) at its output. This approach of rectifying and integrating became widespread since it is possible to make these calculations accurately and inexpensively with the limited electronics technology of earlier decades. Equation (2.2) shows how the calculation of the integrated rectified signal is

done. The advances made in electronics devices during the past decades have made it possible to conveniently and accurately calculate the root-mean-squared (RMS) and the average rectified (AVR) value of the EMG signal. Equations (2.3) and (2.4) shows how the calculation of the RMS and the AVR is done mathematically. The AVR value is similar to the integrated rectified value, if the calculations are made correctly and accurately. The RMS value is a measure of the power of the signal, thus it has a clear physical meaning. For this reason, the RMS value is preferred for most applications [Luc02].

$$x_{IR} = \overline{|x|} = \frac{1}{T} \int_0^T |x(t)| dt \quad (2.2)$$

$$x_{RMS} = \sqrt{\frac{1}{N} \sum_{i=1}^N x_i^2} \quad (2.3)$$

$$x_{AVR} = \overline{|x|} = \frac{1}{N} \sum_{i=1}^N |x_i| \quad (2.4)$$

All of the algorithms mentioned here are some form of an Envelope Follower. The outcome, expressed in microvolt \* seconds, is related to the tension or force exerted by the muscle [DL97]. A commonly used procedure is smoothing the EMG signal by passing the rectified EMG signal through a low-pass filter. This can be done online using an analog device or a digital routine after analog-digital converting. This routine is often called a "contour-following integrator" [Fri09].

### 3 Hardware Implementation

#### 3.1 Approach in Concept and Design

The system proposed in this work is detecting SEMG signals using wet, reusable electrodes with conductive gel placed on the muscle. To make it easier to apply and remove the electrodes, these are integrated into a elastic VELCRO strap similar to the strap Knapp and Lusted used in their "Biomuse" project in 1990 [RBK90].

The connection of the electrodes to the processing stage can be realized in different ways. In [Koc07] and [TSSB08] unshielded cables are used. In [RBK90] and [Wei06] shielded cable are used. Shielded cables in combination with a right leg driver (RLD) circuit reduces common-mode interference and makes the system immune to interferences caused by cable movement. The human body acts as a reference point (ground) for the amplification circuit. A basic circuit of a RLD, according to the datasheet of the INA118 chip, is shown in figure 3.1. The driver is, and was, previously used only in electro-cardiographs (ECG), which measure the electrical activity in the heart. During ECG sessions, the driver is attached to the right leg, as far away from the heart as possible. Twisting the cables helps in cancelling out electromagnetic interference (EMI) from external sources. In the proposed system, the electrodes are connected

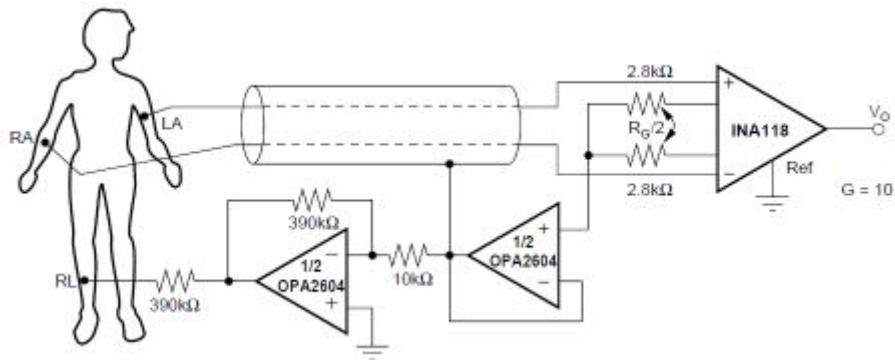


Figure 3.1: Basic red leg driver circuit [BB10]: The two signals entering the instrumentation amplifier are summed, inverted and amplified in the right leg driver before being fed back to an electrode attached to the right leg. The other electrodes pick up this signal and hence the noise is cancelled. The RLD can attenuate mains hum up to 100 times more than the instrumentation amplifier can do by itself.

to an amplification and filter unit (AFU) using high flexible shielded silicon cables. The signals are amplified and analog high-pass filtered. In the next step, an audio interface is used to convert the signals in the digital domain. Filtering, rectifying and detection algorithms were simulated in MATLAB and implemented in Pure Data (PD) for real-time use.

Therefore different tasks and scenarios were developed and applications for artificial and music interaction were designed. In [CIA05], [TKA02] and [GD] the electrodes, the processing and the transmitting unit are combined and placed directly at the recorded muscle. The control signals are transmitted via bluetooth. In contrast to the work of Costanza et al. [CIA05] and [CIAM07] not especially subtle but apparent movements should be detected in this project. When performing with this system on stage the body movements should refer to the produced and sampled sounds.

## 3.2 Development and Implementation

### 3.2.1 Sensor Unit

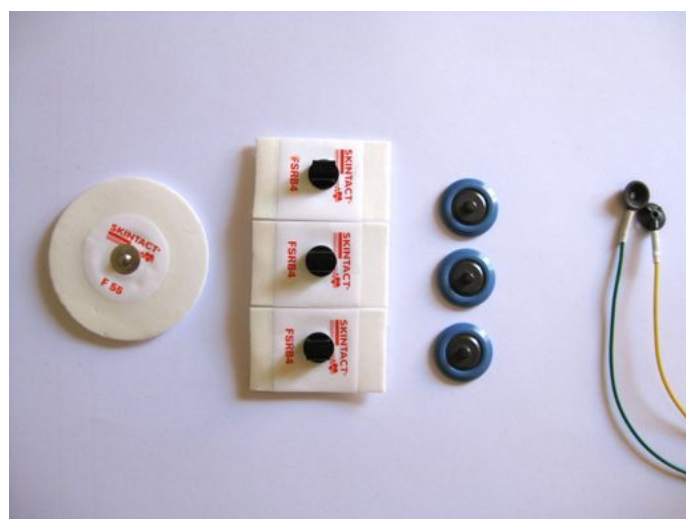


Figure 3.2: The different electrode types that were tested. From left to right: Disposable self-adhesive Skintact wet electrodes, Betterwits reusable electrodes (gel must be applied on the surface), Bio-Sense cup electrodes (gel is used to fill the cavity)

Twisted shielded cables are used for the two input electrodes, to minimise interference caused by cable movements. The reference electrode need not be shielded. Instead of using disposable wet electrodes, three reusable electrodes mounted on a VELCRO strap are used. To achieve a clean signal, a proper skin preparation using skin preparation gel is recommended as well as using conductive gel between the skin and the electrodes.

Different disposable and reusable, self and non-adhesive EMG and ECG (electrocardiogram) electrodes were tested (see figure 3.2) relating to their user friendliness and the achieved signal quality. Reusable Non-adhesive Ag/AgCl snap-on EMG electrodes by BETTERWITTS were chosen. Low intrinsic noise in the electrodes and a good integration in the VELCRO strap provide optimum signal when acquiring data.

### 3.2.2 Amplification and Filter Unit (AFU)

The developed circuit is based on the principal bio sensor circuit with right leg driver shown in figure 3.1. It is shown in figure 3.3.

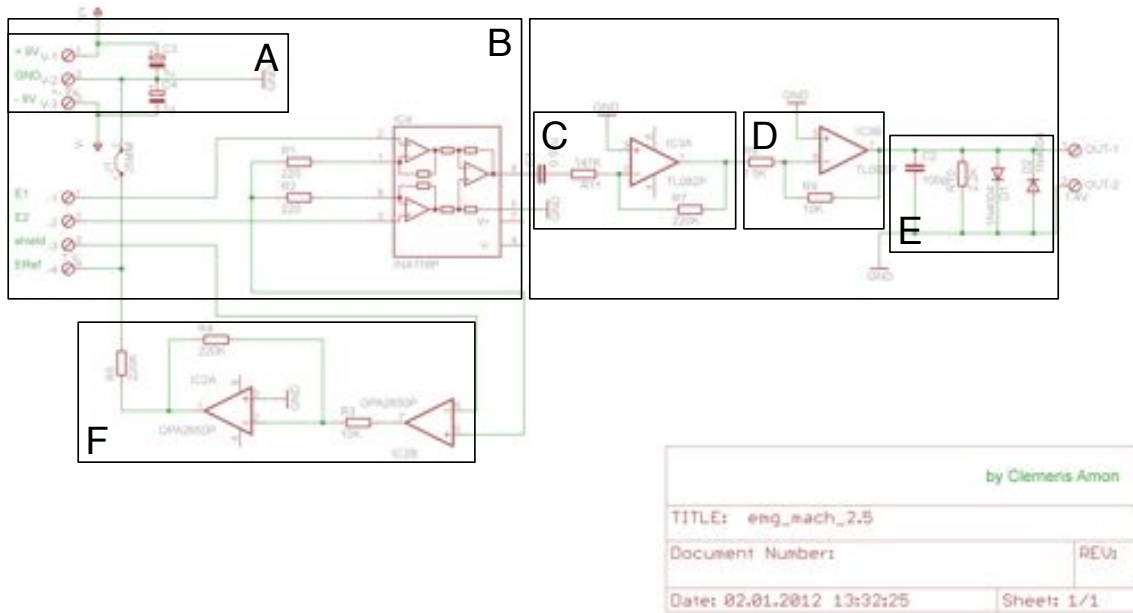


Figure 3.3: Schematics of "EMG Machine"

To achieve the power supply voltage of +/- 9 V two 9 V transistor batteries were used. The positive pole of one battery was connected to the negative pole of the other battery. This results in a virtual ground, and a positive, and a negative 9V pole (see figure 3.3A). The second part of the circuit consists of an integrated circuit (IC) INA118 (see figure 3.3B). It is building the difference between the two input electrodes E1 and E2 and amplifying it by 110. This IC is an instrumentation amplifier whose operation is according to the circuit shown in figure 3.4. This amplifier consists of three operational amplifiers TI082 by Texas Instruments, several resistors R and one gain resistor  $R_{gain}$ . Equation (3.1) shows the transfer function of the used instrumentation amplifier design under the precondition  $R_1=R_2=R_3=R_4=R$ . The instrumentation amplifier can be divided into two stages, the buffer and the differential amplifier stage.

$$V_{out} = (V_1 - V_2)(1 + \frac{2R}{R_{gain}}) \quad (3.1)$$

The operational amplifiers OP1 and OP2 in the first stage operate as buffers. This stage provides a high input impedance, increases the CMRR of the circuit and also enables the buffers to handle much larger common-mode signals without clipping. The two output functions of the first stage are shown in equations (3.2) and (3.3).

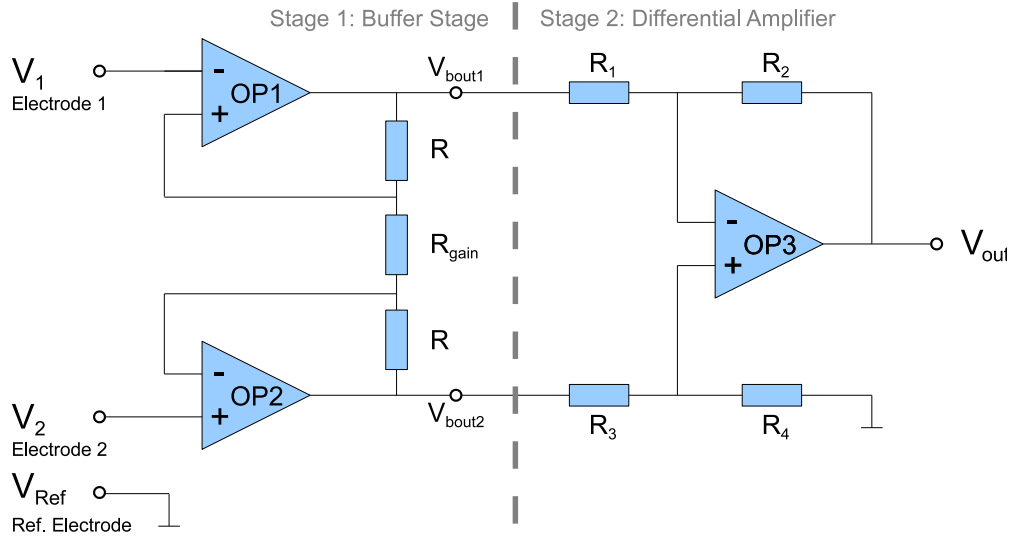


Figure 3.4: Discrete version of an instrumentation amplifier using TI082 operational amplifiers

$$V_{bout1} = V_{dif1} = V_1 \left( \frac{2R}{R_{gain}} + 1 \right) \quad (3.2)$$

$$V_{bout2} = V_{dif2} = V_2 \left( \frac{2R}{R_{gain}} + 1 \right) \quad (3.3)$$

In the second stage a differential amplifier is amplifying the difference of the two inputs signals  $V_1$  and  $V_2$ . The transfer function of the differential amplifier can be calculated by viewing this circuit as a combination of an inverting and a non-inverting operational amplifier. Subfigures 5(a) and 5(b) in figure 3.5 show the two circuits.

In the equations (3.4) and (3.5) the output functions of the two amplifiers are presented. The output  $V_{oinv}$  in equation (3.4) can be derived by driving the first input  $V_{dif1}$  and setting the second input  $V_{dif2}$  to ground. The output  $V_{ononinv}$  in equation (3.5) can be derived by driving  $V_{dif2}$  and setting  $V_{dif1}$  to ground. Simply adding the two parts results in the output function of the differential amplifier. See equation (3.6).

$$V_{oinv} = -V_{dif1} \frac{R_2}{R_1} \quad (3.4)$$

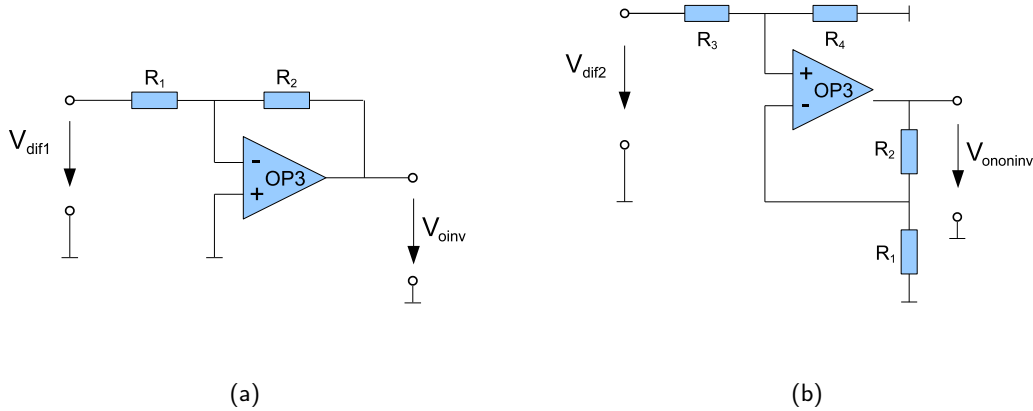


Figure 3.5: The instrumentation amplifier can be seen as a combination of an (a) inverting and a (b) non-inverting operational amplifier.

$$V_{ononinf} = V_{dif2} \frac{R_1 + R_2}{R_1} \cdot \frac{R_4}{R_3 + R_4} \quad (3.5)$$

$$V_{odif} = V_{ononinv} + V_{oinf} = V_{dif2} \frac{R_1 + R_2}{R_1} \cdot \frac{R_4}{R_3 + R_4} - V_{dif1} \frac{R_2}{R_1} \quad (3.6)$$

By choosing  $R_1 = R_3$  and  $R_2 = R_4$  you can specify the gain. This can be seen in equation (3.7):

$$V_{odif} = \frac{R_2}{R_1} \cdot (V_{dif2} - V_{dif1}) \quad (3.7)$$

By choosing  $R_1 = R_2 = R_3 = R_4 = R$  the gain of the whole circuit is set to 1. This can be seen in equation (3.8):

$$V_{odif} = V_{dif2} - V_{dif1} \quad (3.8)$$

Only the difference gets amplified. It can be seen that for common signals at both inputs  $V_{dif1}$  and  $V_{dif2}$  the output  $V_{odif}$  should be zero. This common mode rejection ratio (CMRR), also described in section 2.2.1, is useful but not perfect. It depends on the operational amplifier device itself and on the matching of the resistor values.

In the AFU the gain of the INA118 is set to 110 by choosing  $R_1=R_2=220\ \Omega$ . Equation (3.9) shown how this is calculated:

$$G_{ina} = 1 + \frac{50k\Omega}{R_1 + R_2} \quad (3.9)$$

The INA118 chip has a very high CMRR especially with high gain. A gain of 110 is used in the AFU which eliminates most noise seen by the cables. Table 3.1 shows an extract of the INA118 data sheet where the CMRR dependent on the gain is listed. A CMRR above 120 dB is obtainable. It's impossible to completely eliminate motion artifacts in surface electromyography due to the inherent nature of surface electrodes. The INA118 was integrated in the circuit according to figure 3.3B.

Table 3.1: Common-Mode Rejection INA118

PARAMETER	CONDITIONS	MIN	TYP	MAX	UNITS
Common-Mode Rejection	$V_{CM} = \pm 10V, \Delta R_S = 1kW$				
	G=1	80	90	73	dB
	G=10	97	110	89	dB
	G = 100	107	<u>120</u>	98	dB
	G = 1000	110	125	100	dB

The circuit is complemented by an inverting active high-pass filter with  $f_g=106Hz$  and with a gain of 1.5, see figure 3.3C. This was implemented using a TL082 IC to get rid of movement and surface artifacts, to reduce the 50Hz hum and eliminate any DC offset. Following another active operational amplifier with a gain of 6.6 is used to invert and amplify the signal again and to get a phase of 0 degree, see figure 3.3D. The total gain is now set to 1130. A passive limiter terminates the output voltage to  $\pm 0.6V$  (-5.3dBu) and protects the connected sound card, see figure 3.3E.

To guarantee a constant ground level and to avoid overswing of voltage an active ground circuit in combination with a right leg driver (RLD) was used, see figure 3.3F. The right leg driver circuit is realised using an IC OPA2650. This component is often added to biological signal amplifiers to reduce Common-mode interference [Ach11]. See section 2.2.1 for detailed description of the RLD. The full schematic and the PCB layout which was designed in CadSoft EAGLE PCB Design Software is illustrated in figure 3.3 and appendix C.1.

A small PCB was designed and etched using the laser printer technique. Figure 3.6 shows the PCB design etched but not drilled yet. The dimensions of the PCB and the housing are listed in the table 3.2. A light and small housing made of plastic was used.

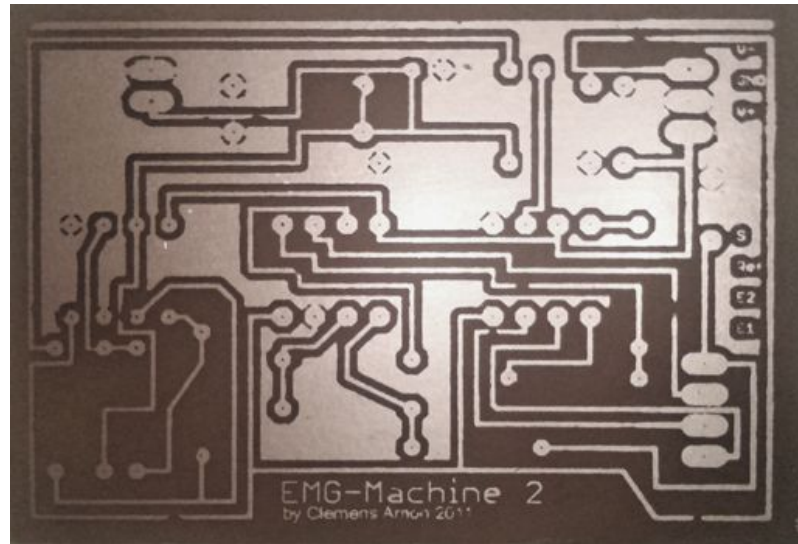
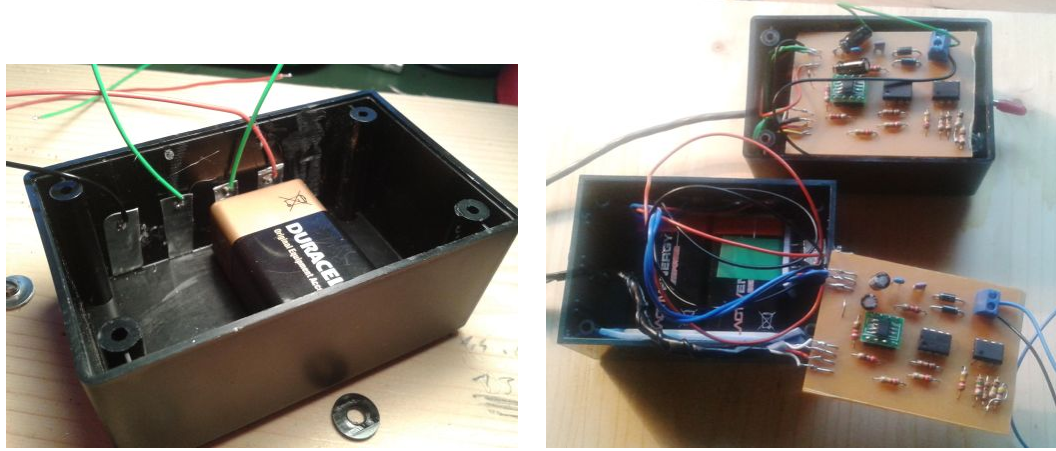


Figure 3.6: Etched printed circuit board, not drilled

Table 3.2: Dimensions: PCB and the housing of the AFU

Dimension	AFU
PCB Length	60mm
PCB Width	40mm
PCB Height	3mm
Housing Length	100mm
Housing Width	45mm
Housing Height	30mm

The two nine-volt transistor batteries are integrated into the housing. The PCB populated with electronic components is placed above the batteries. A picture of the integration of the power supply is shown in figure 7(a). Figure 7(b) shows the built-in populated PCB.



(a) Plastic Housing of "EMG-Machine" with integrated power supply (b) Plastic Housing of "EMG-Machine" with integrated power supply and populated PCB

### 3.3 Reliability, Annoyances - Discussion

The three cables that connect the strap to the amplifier and filter unit could cause annoyance. These cables have to be fixed to the body. (e.g.: from the forearm to the upper arm to the shoulder to the side thorax and to the hip or belt where the amplification and filtering unit is fixed). If the cables are fixed properly large movements (like moving the hand around the head) are possible.

Mobile phones close the the cables or to the EMG Machine causes a noticeable hum in the sensor signal and a lower SNR.



Figure 3.7: An illustration of the developed system

## 4 Theory in EMG Signal Processing

### 4.1 Notch and band-pass filtering

The signal is processed using an Infinite Impulse Response (IIR) notch filter that reduce the 50 Hz Hum followed by a Finite Impulse Response (FIR) band-pass filter to delimit the signal to a useful range and filter out noise in high frequencies. The IIR filter bandwidth is quite narrow (10 Hz) and has a small effect on the signal energy. This filtering is performed in addition to the one implemented in the hardware device because of its higher order and accordingly higher attenuation and sharper cutoff. Figure 4.1 shows the digitally unfiltered raw signal compared to the notch and band-pass filtered signal in the frequency domain. A high reduction of the 50 Hz component can be seen. The blue range marks the signal portion that is analyzed by the Fast Fourier Transform (FFT). The analysis window is purposely set to a region where no muscle activity occurs to show the impact of the filter better. In figure 4.2 the unfiltered and filtered signal is shown as a spectrogram plot where the hum reduction can also be seen very clearly. The reduction can also be seen in the decrease of the ripple in the time signal where no muscle activity is seen (figure 4.3).

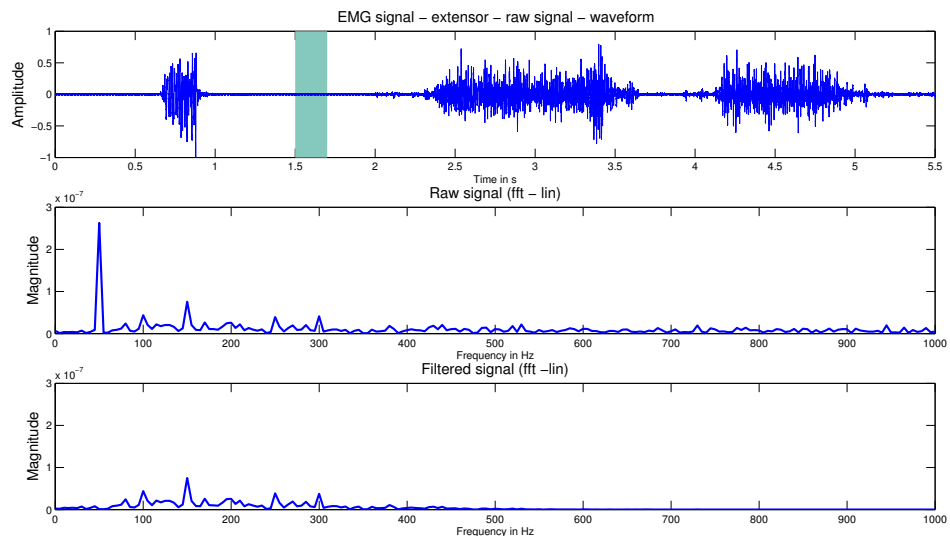


Figure 4.1: Filtered signal: (1) raw time signal with fft window marked,  
(2) corresponding fft plot, (3) fft plot of the filtered signal

In the simulation the band-pass filter is realized using one high-pass and one low-pass filter to test different orders and filter types for each filter. The high-pass filter has a cutoff frequency of  $f_c=5$  Hz and an order of  $N=60$ . The low-pass filter has a cutoff frequency of  $f_c=400$  Hz and an order of  $N=10$ . In the final filtering routine a FIR Butterworth band-pass filter is implemented due to a lower ripple and a better cut-off frequency behaviour.

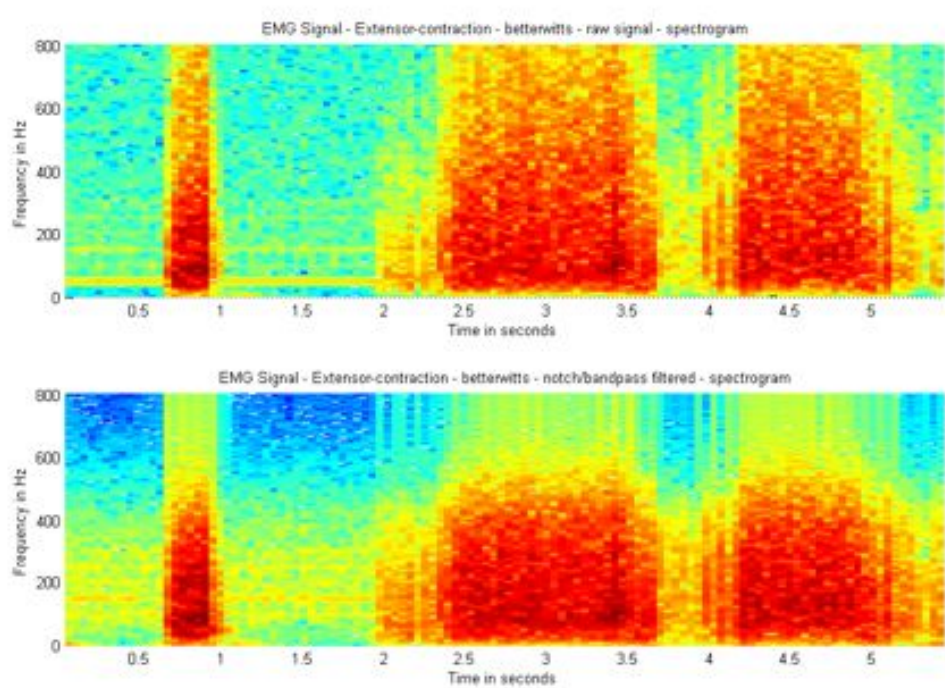


Figure 4.2: filtered signal: (1) spectrogram of the raw signal, (2) spectrogram of the notch and band-pass filtered signal

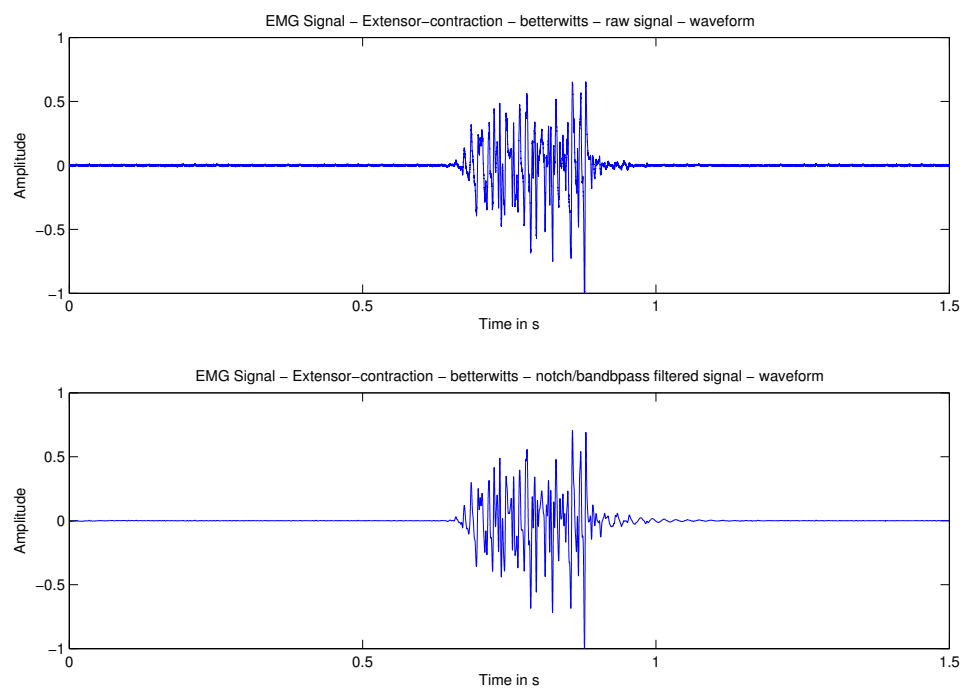


Figure 4.3: Filtered signal: (1) raw time signal, (2) notch and band-pass filtered time signal

## 4.2 Rectification and Smoothing

As mentioned in section 2.5 the RMS value is preferred for most applications in EMG to estimate the amplitude because it reflects the energy of the physiological activities in the motor unit during contraction. In this section, four different methods for rectifying and smoothing the signal are simulated and implemented in MATLAB. For all following calculations the notch and band-pass filtered signal serves as input signal. Table 4.1 lists the four filter and rectification modes proposed in this project. A good combination method should minimize the fluctuations of the signals amplitude. Figure 4.4 shows a comparison of the four proposed combinations of rectifying and smoothing algorithms. In the first graph the absolute values (full-wave rectification, blue) are presented. In graph number two a 10 Hz low-pass filter is applied on the absolute values. A well smoothed signal can be achieved using this method. The Hilbert transform offers another option to rectify and smooth the signal. Equation (4.1) shows how the calculation is done.

$$\hat{x}(t) = |H \{x(t)\}| \quad (4.1)$$

Graph three and four in figure 4.4 show how the raw and the low-pass filtered hilbert transformed signal looks like the time domain. In figure 4.5 the hilbert transformed signal  $x(t)$  is compared to the rectified signal (full-wave rectification). It can be seen the the Hilbert Transform algorithm acts like a envelope follower and hence as shown in figure 4.6 will give a higher amplitude after the low-pass filtering. The hilbert transformed and butterworth low-pass filtered signal with a cutoff frequency of  $f_c=10$  Hz and an order of  $N=4$  is smoothed quite well but shows a small undershoot. The shape of the filtered full-wave rectified signal is similar to the filtered Hilbert transformed signal.

Table 4.1: Evaluated modes processing the signal

Mode No.	Description
1	Absolute values
2	Absolute values + LP filtered [10Hz, IIR, win: BW, filter order n=4]
3	Hilbert
4	Hilbert + LP filtered [10Hz, IIR, win: BW, filter order n=4]

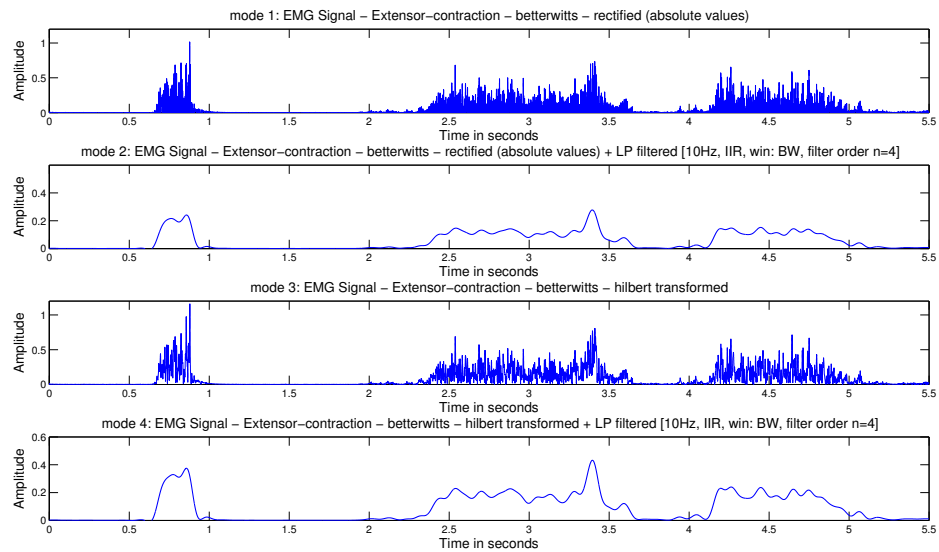


Figure 4.4: (1) mode 1: Absolute values, (2) mode 2: Absolute values + LP [10Hz], (3) mode 3: Hilbert transformed, (4) mode 4: Hilbert transformed + LP [10Hz]

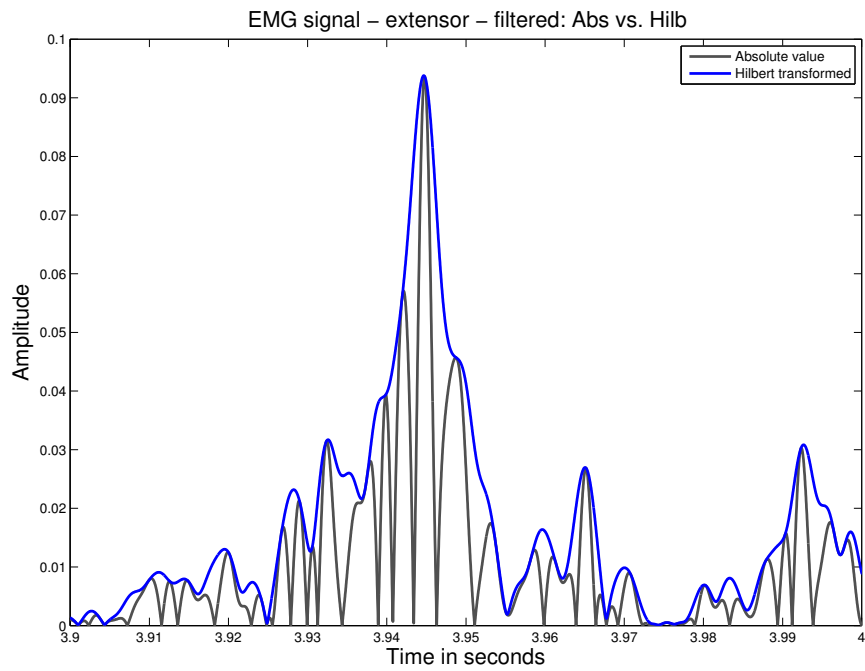


Figure 4.5: Absolute values of the signal (simple rectification) and hilbert transformed signal

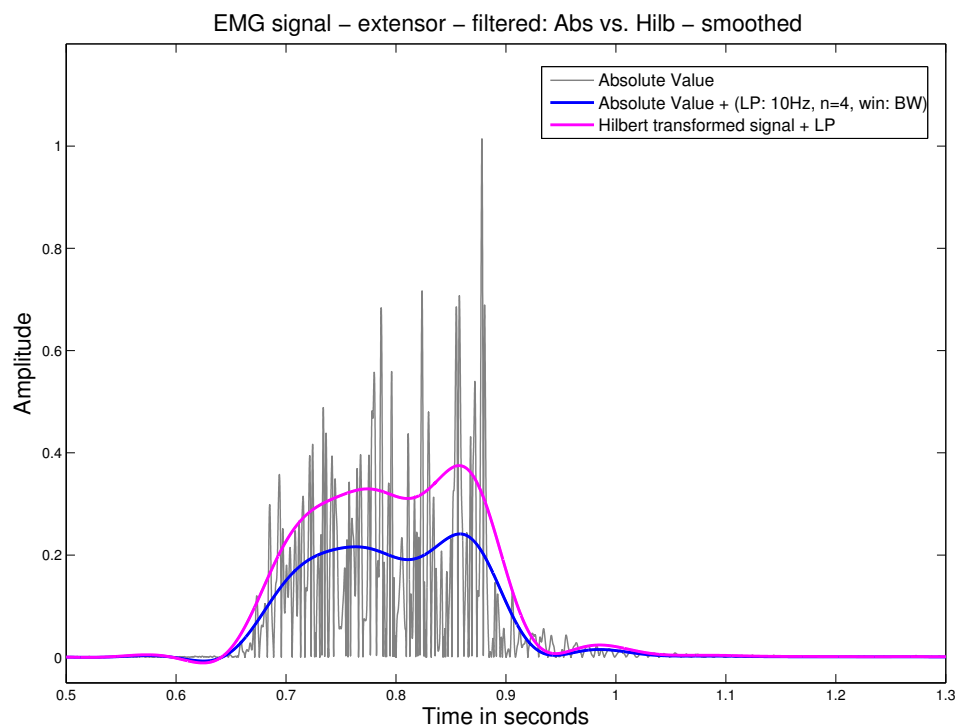


Figure 4.6: Absolute values of the signal and hilbert transformed signal - both LP filtered: [10Hz, IIR, win: BW, filter order n=4]

### 4.3 Signal Detection Theory

The Signal Detection Theory (SDT) offers a fundamental way for decision making, including a precise language and graphic notation. The theory is often used in sensory experiments to show how well a signal can be detected or extracted in a noisy surrounding. In the following chapters important ideas from signal detection theory are presented that build the fundament for further evaluation of the conducted user study.

#### 4.3.1 Probability Density Function (PDF)

Figure 4.7 shows the PDF of the noise (on the left side) and the signal + noise (on the right). Here the signal in respect to EMG is the signal that is recorded when force is produced by the muscle. Noise is the signal acquired by the electrodes when no muscle contractions are performed. The PDF curves describe the likelihood for the signals amplitude to take on a certain value.

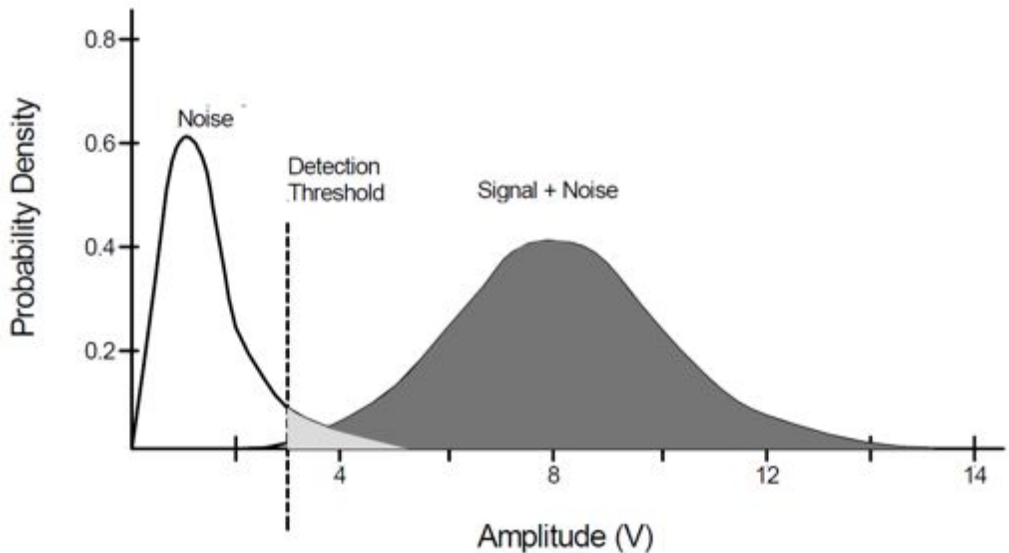


Figure 4.7: Histogram of Noise and Signal+Noise

It is common for probability density functions to be parametrized in terms of the mean  $\mu$  and the variance  $\sigma^2$ . In the field of EMG two types of PDFs are important: The normal (or Gaussian) distribution [Tan12], a continuous probability distribution, defined by

$$f(x) = \frac{1}{\sigma\sqrt{2\pi}} e^{-\frac{(x-\mu)^2}{2\sigma^2}} \quad (4.2)$$

and the Rayleigh distribution, a continuous probability distribution for positive-valued random variables which occur by rectifying the EMG signal. The Rayleigh distribution [Pro85] is given by

$$f(x; \sigma) = \frac{x}{\sigma^2} e^{-x^2/2\sigma^2}, x \geq 0 \quad (4.3)$$

There is a region where the curves of the signal and the noise overlap. Here it's not possible to decide if the actual amplitude value is part of the signal + noise or not. By setting a threshold the signal + noise can be separated from the noise. To find a suitable threshold the false alarm and hit rates for the two signals can be calculated. A false alarm occurs when the noise signal exceeds a predefined threshold. The Probability of a false alarm is given by

$$P_{fa} = \frac{\sum_{k=1}^N t_k}{T_k} \quad (4.4)$$

where  $t_k$  is the time the noise envelope is above the threshold as graphically shown in figure 4.8 and  $T_k$  is the total time [Bro07]. Accordingly a hit occurs when the signal + noise exceeds the predefined threshold.

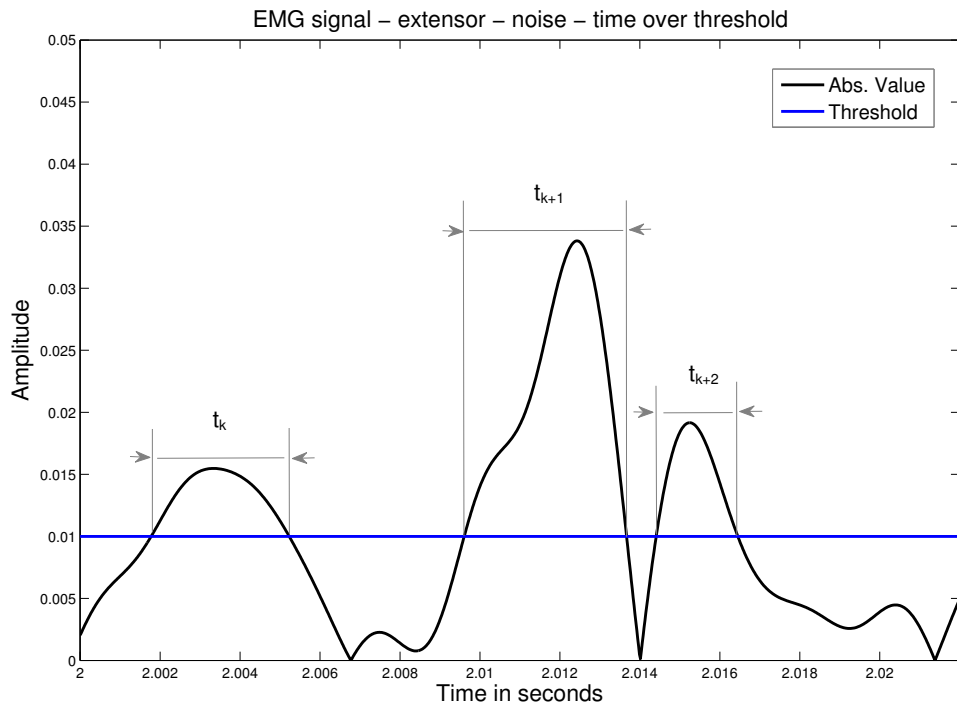


Figure 4.8: Estimated time above threshold

$P_{fa}$  can be easily calculated in MATLAB using the function in listing 1 below. Running this function in a loop for thresholds from 0% to 100% of the maximum amplitude provides a set of false alarm rates, in the case of noise used as input signal, or hit rates, in the case of recorded contractions used as input signal. The quality of detection can be shown by plotting the Receiver Operating Characteristics (ROC) curve. This basic classifier is called Single Threshold Detection (STD).

Listing 1: MATLAB source code: calculation of time over threshold

```

1 % input parameters:      s ... signal
2 %                           th ... threshold
3 % output parameter:      t ... time over th in relation to total time
4
5 function t = time_over_threshold(s,th)
6
7 signal = zeros(size(s));
8 signal(find(s≥th)) = 1;
9 t = length(find(signal==1))/length(s);
10
11 end

```

#### 4.3.2 Receiver Operating Characteristics

A Receiver Operating Characteristics (ROC) also known as ROC curve is a graphical plot of the fractions of the false alarm rate vs. the hit rate at different thresholds. Under the assumptions of signal detection theory interpolating the points for the different values of the threshold leads to a curve. As shown in figure 4.9 the shape of the curve changes as the sensitivity  $d'$  (also called discriminability index) changes. This index depends on the separation and the spread of the noise-alone and signal + noise curves in the histogram and is given by the simple formula (4.5) [Hee98].

$$d' = \frac{\text{separation}}{\text{spread}} \quad (4.5)$$

These two parameters and consequently  $d'$  depends on the signal strengths and on the various rectifying and filtering methods applied on the signal. When the signal is stronger or due to filtering the ripple of the amplitude is reduced the overlap of the two histogram curves becomes less and the ROC curve becomes more bowed. Another definition of the sensitivity can be found in [MC04]. Here  $d'$  is given as shown in formula (4.6).

$$d' = z(H) - z(F) \quad (4.6)$$

where  $z(H)$  and  $z(F)$  are the inverses of the cumulative Gaussian distribution of the hit and the false alarm rate. These inverses can be calculated using MATLAB's 'norminv' function. A higher  $d'$  indicates that the signal can be detected more reliably.

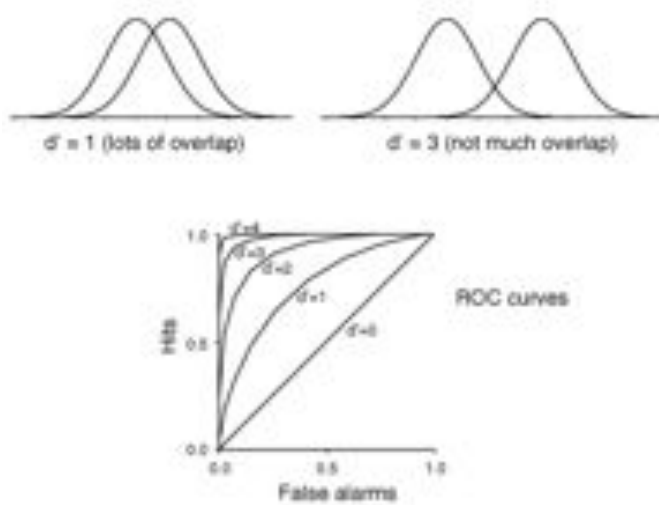


Figure 4.9: A Receiver Operating Characteristics [Hee98]

### 4.3.3 Double Threshold Detection

The double threshold detection (DTD) algorithm works as a combination of two single thresholds. This method is detecting an overstep only when the signal is falling below a certain second threshold that is set to a lower amplitude level than the first one. To avoid unwanted loss of detection due to small variations in the muscle force the lower second threshold is integrated. So the DTD is an improved method of the STD. Figure 4.10 shows how this algorithm works and which time ranges of  $t_k$  are chosen to calculate the hit rate.

Here the upper threshold  $Th_{up}$  is set to 0.235 (72% of the maximum amplitude) and the lower threshold  $Th_{lo}$  is set to 0.17 (42% of the maximum amplitude). The detection time is defined as the time between the first crossing of the signal and  $Th_{up}$  and the second crossing of the signal and  $Th_{lo}$ . False alarm rate  $P_{fa}$  and hit rate  $P_h$  are calculated in MATLAB using the function in listing 2 below.

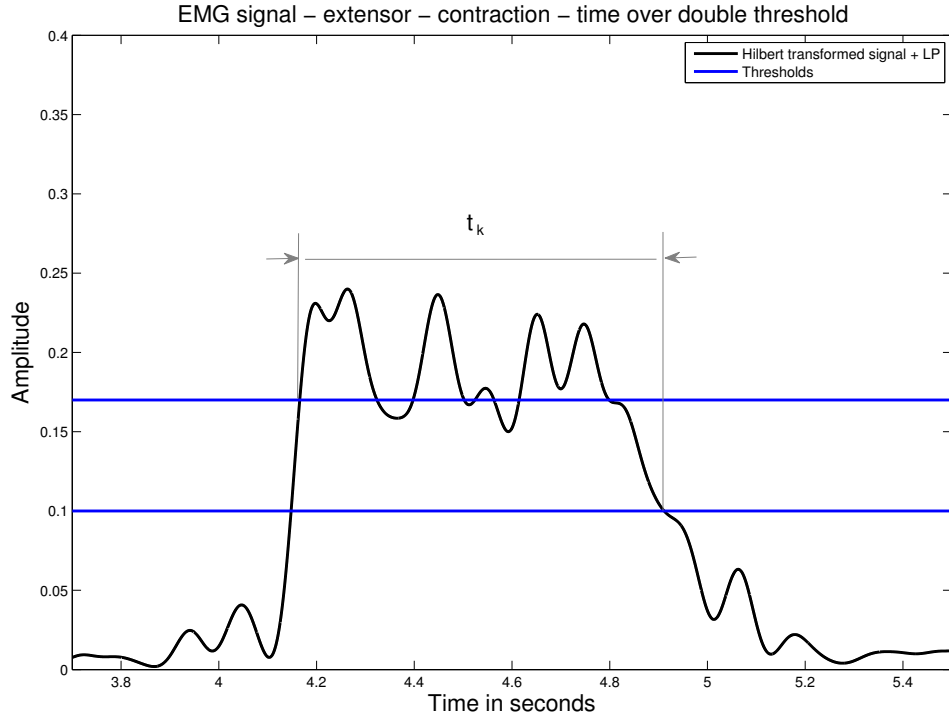


Figure 4.10: Estimated time above threshold for DTD

Listing 2: MATLAB source code: calculation of time over double threshold

```

1 % input parameters:      s ... signal
2 %
3 % output parameter:      t ... time over th in relation to total time
4
5 function t = time_over_doublethreshold(s,th)
6 signal_up = s;
7 signal_do = s;
8 signal_up(signal_up≥th) = 1;           % threshold 1 (upper th)
9 signal_up(signal_up

```

```
19 ds_nz(ds_nz==0)=[];
20 ds_nz_neu=[ds_nz;0]+[0;ds_nz]; % no zero + no zero shift sum by one ...
    point
21 ds_begin=find(ds_nz_new==2); % index of start points within the ...
    detection vector
22 ds_stop=find(ds_nz_new== -2); % index of stop points within the ...
    detection vector
23 ds_pos=(find(ds==1|ds== -1|ds==2|ds== -2)); %find all crossing points
24
25 % 100% detection workaround (third event becomes second event)
26 if max(ds_stop) > length(ds_pos)
27 ds_stop = ds_stop -1;
28 end
29 % find start/stop samplepoints
30 ds_pos_begin=ds_pos(ds_begin,:);
31 ds_pos_stop=ds_pos(ds_stop,:);
32 % calculate sum of times over th and divide it by the signal length
33 t = sum(ds_pos_stop - ds_pos_begin)/length(s);
34 end
```

## 5 Evaluation

In the next sections the four modes of rectification and smoothing are simulated and tested in MATLAB using recordings of 6 different subjects which were made during a user study.

### 5.1 User Study

Recordings of EMG-signals of different people were made to collect data for evaluation. Four tests were designed and were completed by six subjects. The sensor strap was located at the forearm and the task was to press a small soft ball when acoustic stimuli played over headphones were heard. The subjects were first introduced to the four test scenarios and didn't get any visual feedback except in test 3 where the sweep ramp and the actual time position were displayed. The random sequences and test scenarios (note on, note off, velocity, midinote) were programmed and exported as midi files using the MATLAB function 'writemidi.m'.

#### 5.1.1 Test 1

The test duration was 4 minutes (240s). 24 audio stimuli randomly distributed over time were played during the test duration. Stimulus characteristics: 500 Hz sinus in 6 different durations each played 4times (100ms, 200ms, 500ms, 1000ms, 2000ms, 5000ms). The subject is asked to perform maximum contractions (full power instruction). Start times and stimulus durations were saved for analysing. EMG-signals were recorded.

#### 5.1.2 Test 2a

The subject hears the tonescale of C major from C3 to C4 and back (16 tones). Tone playback duration is 2 seconds per tone with breaks of 2 seconds between the single sinusoidal tones. The subject is asked to do contractions (press the soft ball) with the force corresponding to the tone and then stop the contraction and relax till the next tone starts. The lower C represented the minimum force possible and the higher tone c represents the maximum force. The idea was to test the sensitive with which people can control their muscle activity.

#### 5.1.3 Test 2b

Test 2b is the continuous version of 2a. The sinusoidal stimulus tone starts at a frequency of 130,813 Hz (C3) and rises to 261,626 Hz (C4) and then back to C3 in a duration of 24 seconds. The subject should follow the frequency by pressing the ball with the force corresponding to the actual tone frequency. Again the lower C3 should represent the minimum force possible and C4 should represent the maximum force.

## 5.2 Evaluation Results

All these recordings were used to evaluate the four processing modes (see table 4.1) and compare the STD and the DTD algorithm (see Section 4.3). This was done both for test 1, where subjects were asked to do contractions with maximum force, and for tests 2a and 2b in which subjects were asked to do contractions with variable amounts of force. To achieve this, hit and false alarm rates for the tests, the four modes and the two algorithms were calculated at different thresholds and then sensitivity was estimated. The threshold steps were defined in fractions of the maximum contraction amplitude of each subject.

In figures 5.1 the probability density function of test 1 is presented for the unsmoothed (mode 1 and 3) and smoothed (mode 2 and 4) signals. It is evident that the separation of the contraction signal + noise and the noise gets higher when low-pass filtering is used. The separation in mode 4 is the highest of all four modes. It also can be seen that according to [Bro07] the distribution changes after the rectification to a Rayleigh distribution, also explained in section 4.3.1. The hit rate and false alarm rates of each of the six subjects that participated in test 1 are presented in figure 5.2 and figure 5.3. The false alarm rates were calculated using 20 seconds of noise of each subject. The step size is set to 0.2% what means that 500 values are calculated for each analysed file. In the figures, the x-axis is limited from 0% to 20% to zoom in to the interesting range at lower thresholds and the mean value is plotted in black.  $\text{Th}_{\text{up}}$  is going from 0% to 100% of the subject's maximum contraction amplitude.  $\text{Th}_{\text{do}}$  is set to be  $0.2 * \text{Th}_{\text{up}}$  for each step. It can be seen that the noise amplitude is low compared to the amplitude of the contractions. Thus the false alarm rate is approaching zero at a very low threshold. The more the signal is smoothed by low-pass filtering the wider the curve becomes. Filtering results in a broadening of the useful area for the hit rates as well, as hit rates remains high for a larger threshold interval. A similar trend was observed in the other tests case and the double detection algorithm, with detection in the low-pass filtered modes yielding broader curves and better separation of noise and signal.

Following, ROC curves were estimated for test 1 STD algorithm (see figure 5.4), test 1 DTD algorithm (see figure 5.5), test 2 STD algorithm (see figure 5.6) and test 2 DTD (see figure 5.7). As there was continuous contraction of variable force in test 2a in contrast to test 1 where discrete contractions of maximum force were performed, a better picture about how the algorithms behave in different conditions can be obtained. In all cases false alarm rates were estimated using the noise signal in the areas of test 2b where no muscle contractions were performed.

Average ROC curves were then calculated using the vertical averaging method for ROC curves ([PFK97]). Using this method the curve is vertically sampled in small steps (here 1000) to obtain better resolution. Then the vertical mean of each dataset across the 6 subjects is calculated at each of the 1000 sample points. This vertically averaged curve is showing the average of 6 performance curves. It is intended to provide a comparison measure between

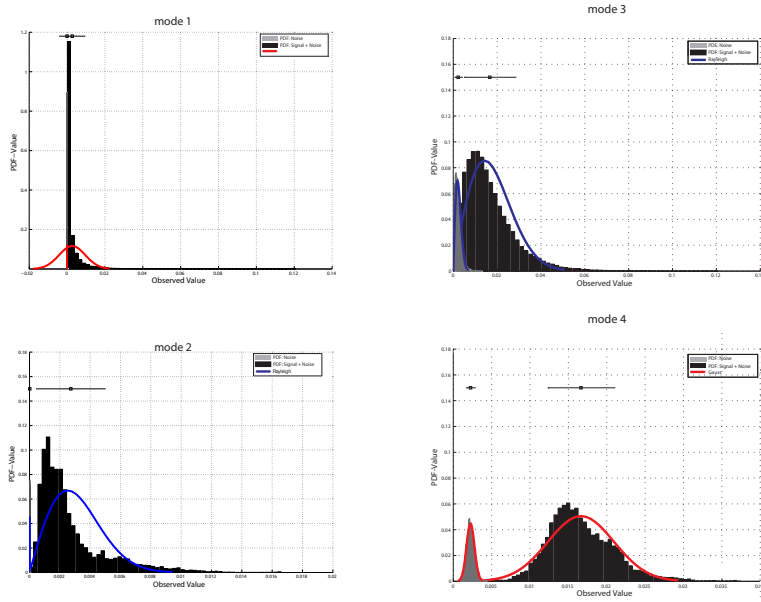


Figure 5.1: Histogram of noise and contraction signals (test 1) of subject 3 for mode 1, 2, 3 and 4.

the different algorithms. An alternative way would be to calculate an average curve based on averaging the hit and false alarm rates across the six users for the same thresholds. The first method was preferred here as the goal is to compare the algorithms and not to provide threshold estimators. That is why this algorithm is chosen in this work. As in this method the curve is averaged only in the y-direction it is the most optimistic way of averaging. Threshold averaging would also provide an informative threshold comparison.

By observing figure 5.8 we can see that the low-pass filtered algorithms perform better than the other two in both tests and both the single and the double detection algorithm. This was clear when observing the histograms, but it is also verified when observing the mean ROC curves. Of the two low-pass filtered algorithms, mode 4 seems to have a small advantage in comparison to mode 2, especially when considering test 2 where contractions of variable intensity were performed. In addition, a small improvement in detection for the DTD algorithm can be seen when comparing the single threshold ROC curves (fig. 5.6) and the double threshold ROC curves (fig. 5.7). A slightly higher hit rate is obtained for the same range of false alarms. This improvement can be verified also in figure 5.8 where the average curves according to the vertical averaging algorithm are plotted for the four modes, the two algorithms and the two tests used in the evaluation.

Finally, the above results are plotted in sensitivity space. Figure 5.9 shows a linear model of the Z-transformed ROC curves, obtained by linear regression on the vertically averaged curve data for all modes and tests. These curves have a slope different than one, because the variance in the noise and contraction signals is not equal (see figure 5.1). In [MC04] MacMillan and

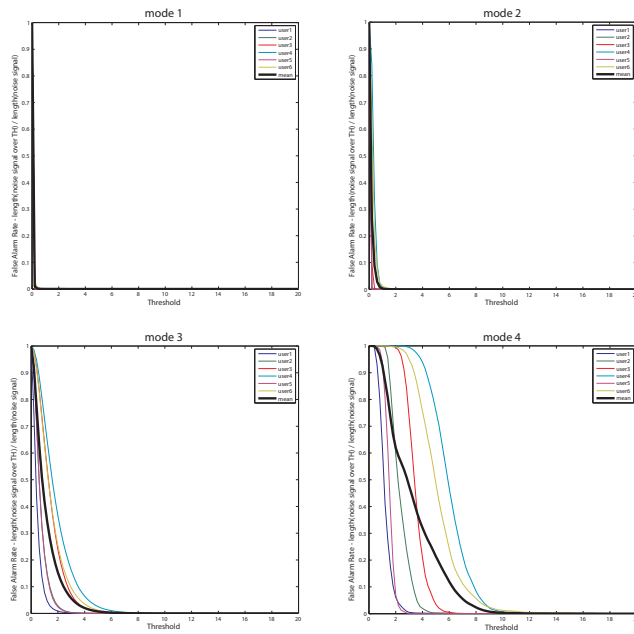


Figure 5.2: False alarm rates vs. threshold steps (test 1, single threshold): (1) mode 1, (2) mode 2, (3) mode 3, (4) mode 4

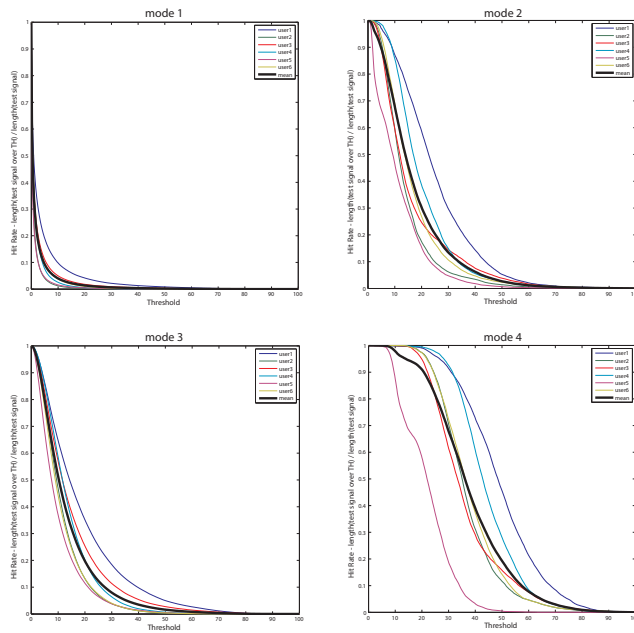


Figure 5.3: Hit rates vs. threshold steps (test 1, single threshold): (1) mode 1, (2) mode 2, (3) mode 3, (4) mode 4

Table 5.1: Values of  $da_2$  and  $d_2$  for all filter and detection modes for test 1 and test 2

Algorithm	Mode	Da2		D2	
		Da2(test 1)	Da2(test 2)	D2(test 1)	D2(test 2)
Single Threshold	I	1.26	0.73	1.00	0.62
	II	4.30	2.44	3.05	1.83
	III	2.88	1.92	2.31	1.59
	IV	5.07	3.17	3.58	2.35
Double Threshold	I	1.65	0.83	1.30	0.69
	II	4.51	2.79	3.26	2.08
	III	3.13	2.24	2.42	1.07
	IV	5.02	3.43	3.55	2.44

Creelman are presenting different methods for calculating the parameter  $d'$  in the case of ROC curves with slope different than one. This parameter is useful as it enables the confirmation of the observations with respect to the performance of the different algorithms and modes.

Based on a model of sensitivity as described in formula (5.1), one first obtains  $d_2$  and  $d_1$ , where  $d_2 = a$ , and  $d_1 = -\frac{a}{b}$ . The slope of the curve  $s$  is then given by  $s = \frac{d_2}{d_1}$ . A single measure of sensitivity for the curve is then given by Equation 5.2:

$$z(H) = a + b * z(FA) \quad (5.1)$$

$$da_2 = \sqrt{\frac{2}{1+s^2}} d_2 \quad (5.2)$$

where  $z(H)$  and  $z(FA)$  represents the z-transformed of the hit and the false alarm ratio and  $a$  and  $b$  are the intercept and the slope of the linear model. Alternatively, one can present the  $d_2$  value. Results are shown in table 5.1 and are also included in figure 5.9 where the  $da_2$  values are presented. The  $d'$  estimators confirm the observations made so far, that is that mode 4 provides best detection in all cases, followed by mode 2, then mode 3 and last mode 1. DTD is providing slightly better detection than STD in most of the cases. Detection was overall worse in test 2 compared to test 1.

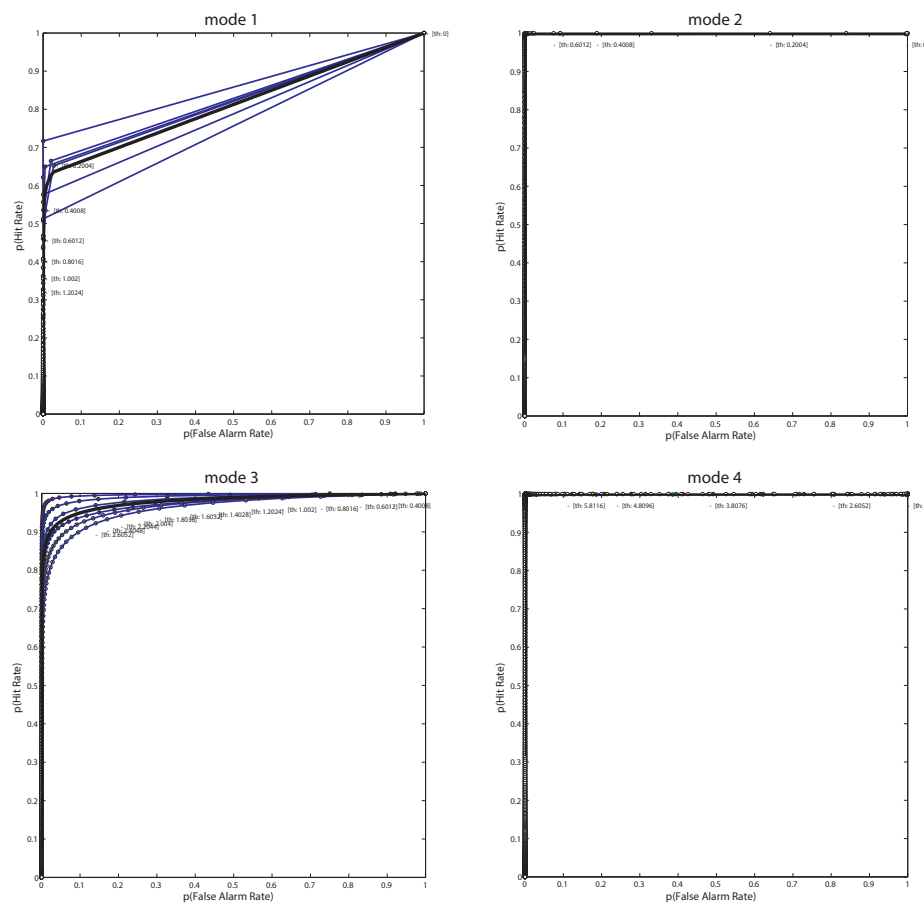


Figure 5.4: ROC curves for all 4 modes: false alarm rates plotted against hit rates (test 1 - STD): (1) mode 1, (2) mode 2, (3) mode 3, (4) mode 4, different lines represent different subjects at all 500 threshold steps tested.

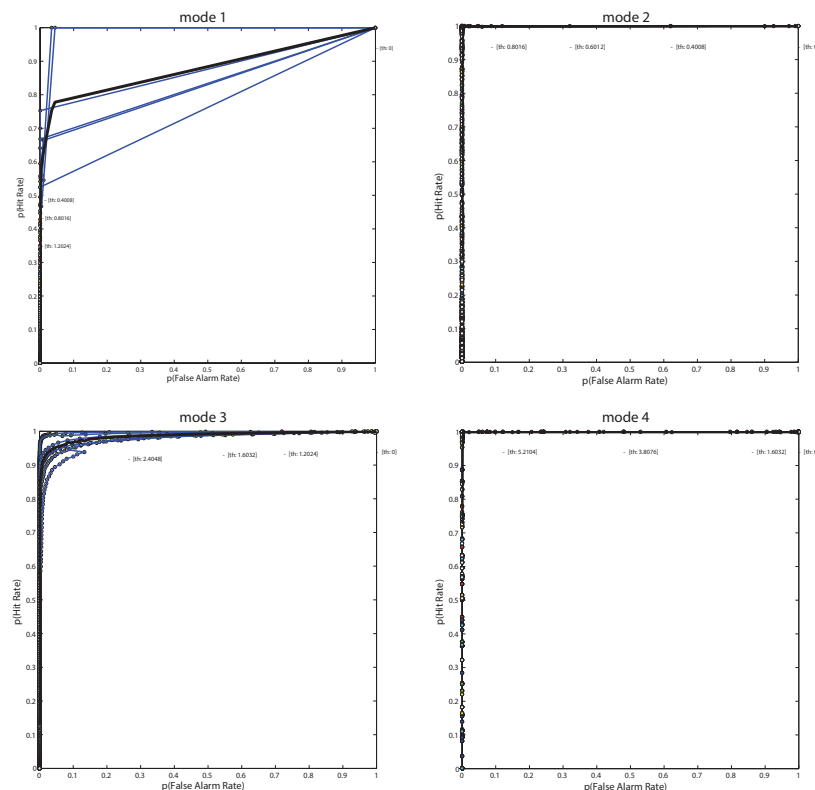


Figure 5.5: ROC curves for all 4 modes: false alarm rates plotted against hit rates (test 1 - DTD): (1) mode 1, (2) mode 2, (3) mode 3, (4) mode 4, different lines represent different subjects at all 500 threshold steps tested.

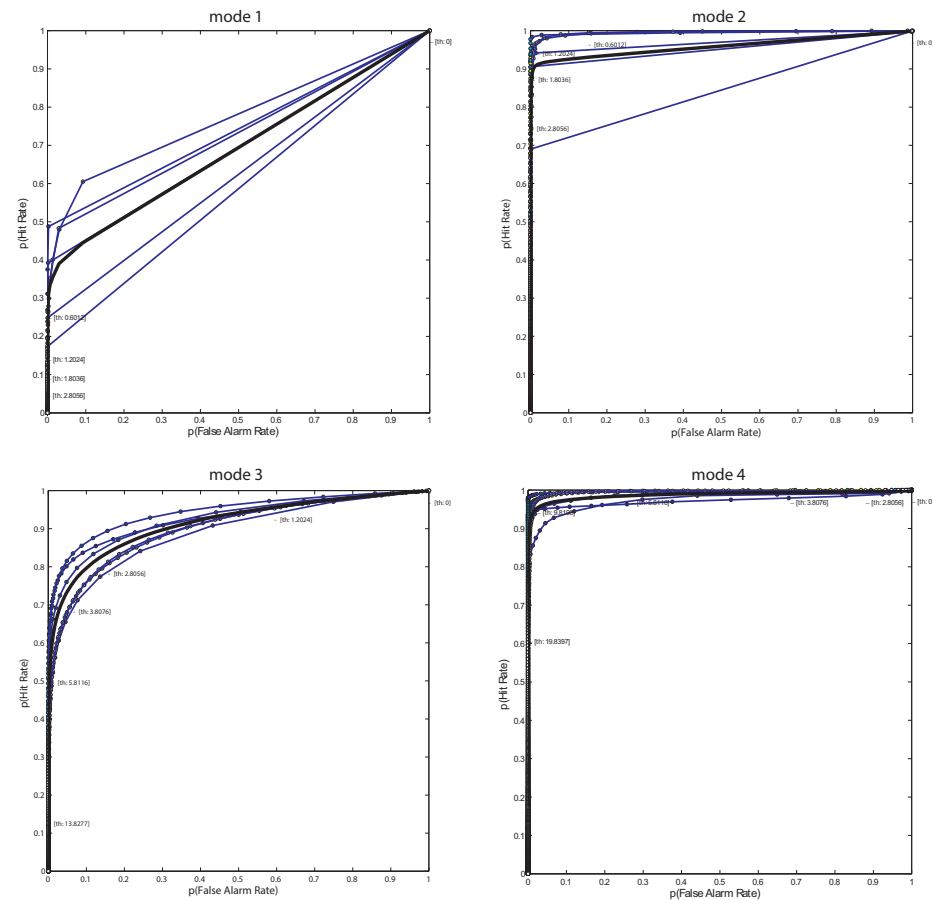


Figure 5.6: ROC curve for all 4 modes - STD, analysed signals: ramp recordings from test 2: (1) mode 1, (2) mode 2, (3) mode 3, (4) mode 4

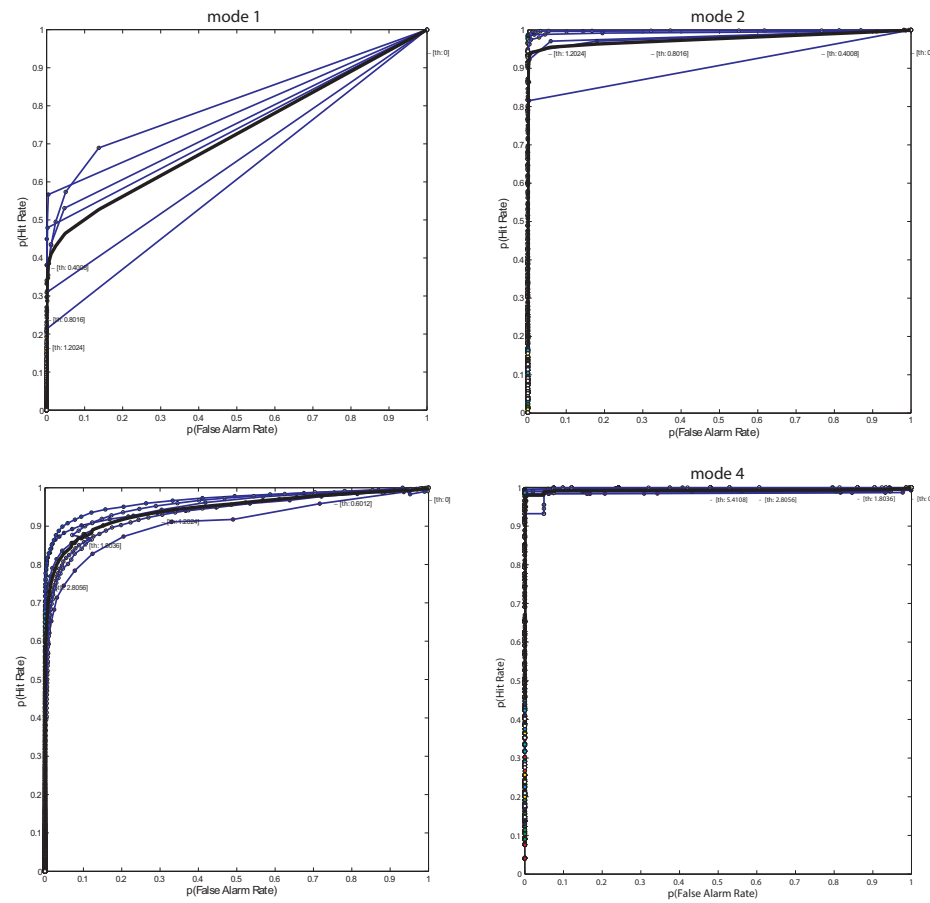


Figure 5.7: ROC curve for all 4 modes - DTD, analysed signals: ramp recordings from test 2: (1) mode 1, (2) mode 2, (3) mode 3, (4) mode 4

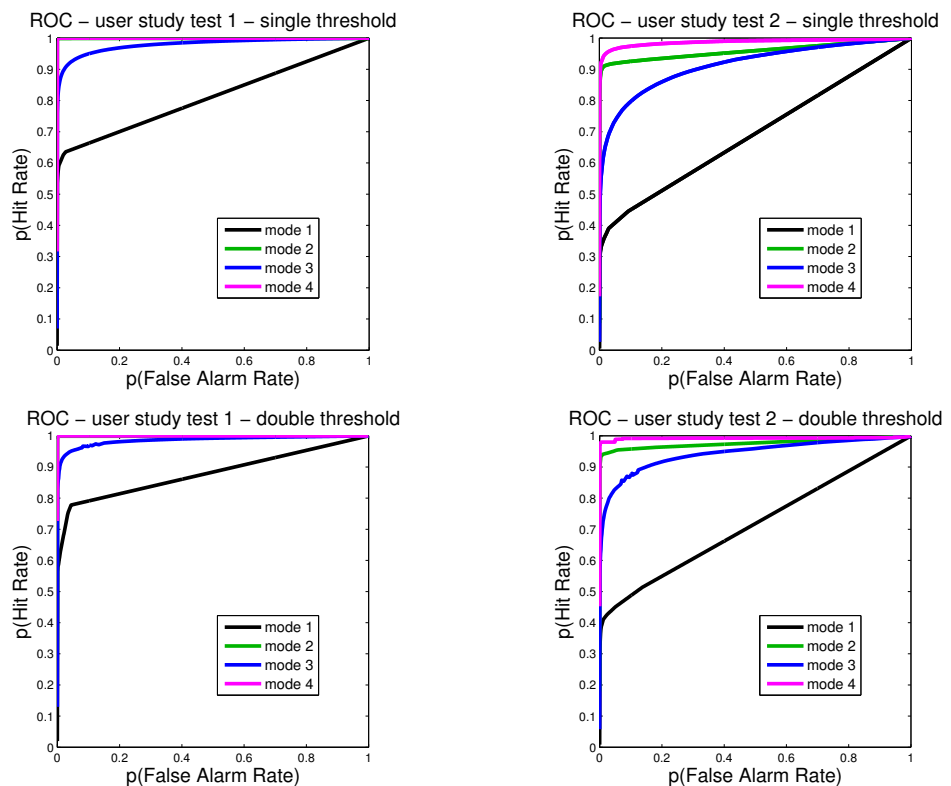


Figure 5.8: Means of ROC curves of all 4 modes analysing recordings of test 1: Up: STD Algorithm, Below: DTD Algorithm, Left: test 1 and Right: test 2

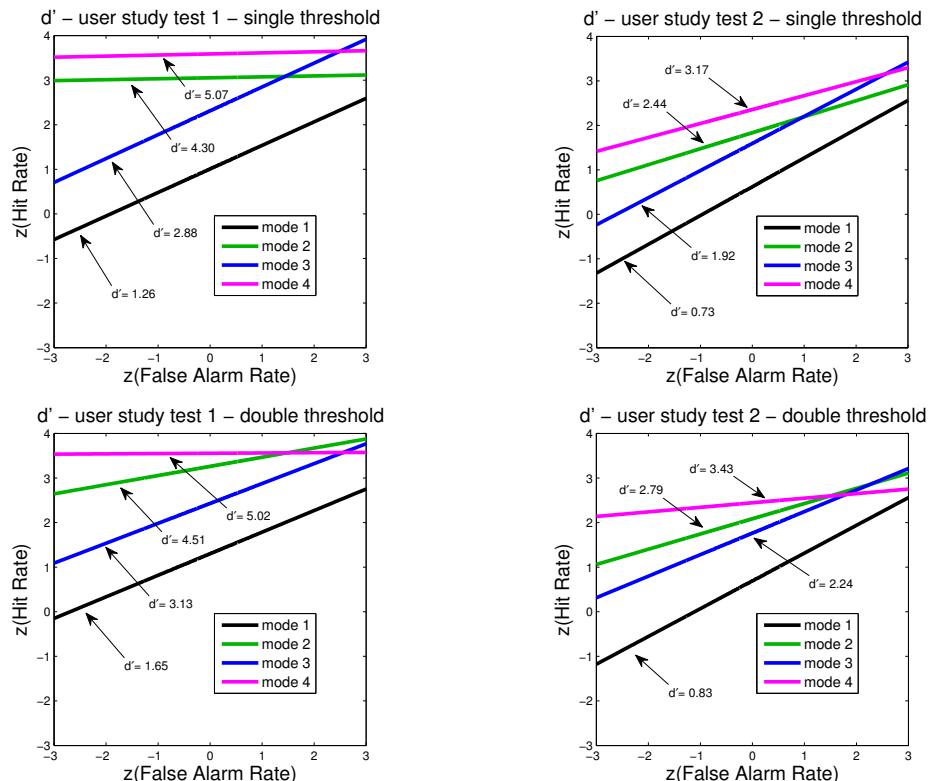


Figure 5.9: Linear regressed sensitivity  $d'$  curves of all 4 modes analysing recordings of test 1 and test 2: Up: STD Algorithm, Below: DTD Algorithm, Left: test 1 and Right: test 2. The values of  $d'$  show that mode 4 results in the best detection.

## 6 Conclusion

In this work, the background concerning bioelectrical signals from muscle activation was researched and presented. Following, a circuit to obtain such signals was designed, created and tested. The circuit can be used in a wearable hardware device for signal acquisition. The resulting hardware was used to obtain bioelectrical signals and four different algorithms for signal pre-processing were implemented. Following a user study was performed to obtain discrete and continuous muscle activation signals of maximum and of variable intensity. These were used to compare four signal preprocessing methods and two simple threshold detection algorithms. The comparison was done using detection theory.

The results show that low-pass filtering the envelope of the bioelectric signal provides a good way for signal preprocessing of muscle activation signals. Obtaining the signal envelope using the Hilbert Transform provides a small advantage compared to simple signal rectification. Finally, the DTD algorithm provides a detection advantage compared to the STD algorithm.

Future works could be directed in further developing the signal circuit by implementing analog-digital conversion (ADC) on the circuit board so that the need for an audio interface or any other ADC device is avoided. As the desired frequency range is small, a lower sampling rate is sufficient. It is further necessary to come up with a way to provide threshold values for different users. This could be achieved using the threshold averaging method. This was not implemented here, but future work should be directed into investigating how robust threshold estimators can be calculated and providing a statistical analysis of the results. More complex classifiers are also a promising future direction so that more complex interaction patterns can be recognized.

### 6.1 The live scenario

The proposed system was tested in an live environment where the start and the length of the playback of two audio samples were triggered by contractions of the user's right and left forearm. The signal processing and DTD algorithm were implemented in the real-time graphical dataflow programming language PURE DATA (PD). It was shown that under controlled settings (e.g.: no body movements except the movements to activate the forearm muscles) the system is working reliably and the sample playback can be controlled well. The GUI (graphical user interface) of this test patch is shown in figure 6.1.

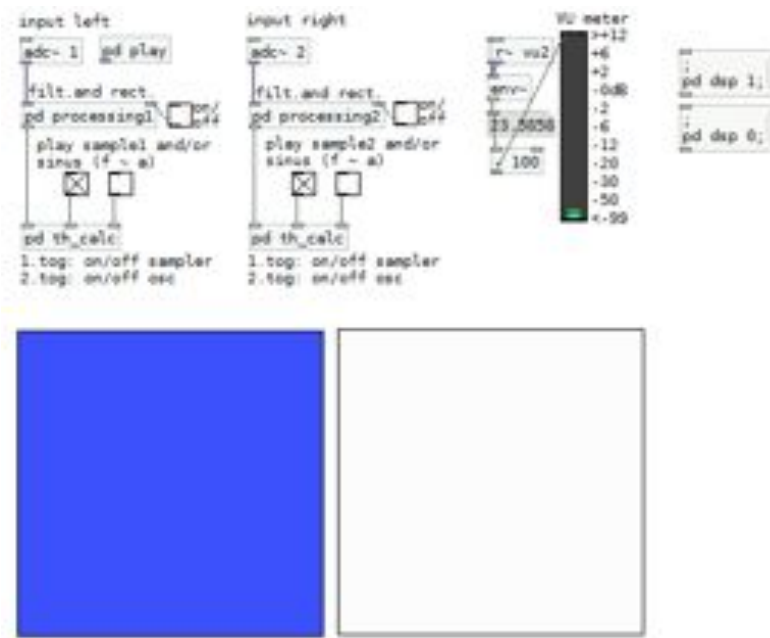


Figure 6.1: GUI of the live application, implemented in Pure Data

## 6.2 Possible Enhancements

### 6.2.1 Hardware

The biggest issue in hardware is it's size and the need of annoying cables. Possible enhancements are the realisation of the amplification and filter unit with ultra-low-power operational amplifiers and the extension of the unit by an analog-digital converter. The whole hardware (amplification and filter unit and the sensor strap) could be merged together to one device worn directly at the muscle. Furthermore wireless technology (e.g.: ZigBee) offers the possibility to transmit the data to the controlled device (music player, sequencer, synthesizer, mobile phone,...).

### 6.2.2 Software

It has to be analysed if an adaptive algorithm to define the threshold is giving better user control. Possible algorithms to evaluate are the Constant False Alarm Rate (CFAR) processor introduced in [Bro07] and the improved method for muscle activation detection during gait by Lanyi X and A. Adler in [XA04]. Decomposing the EMG-signal could offer a method to compare single components of signals measured by different electrodes. This could lead to a system where with one sensor strap located at the forearm the finger movement can be detected (e.g.: the control of amputation appliance, virtual keyboards, virtual devices,...).

## References

- [Ach11] Venkatesh Acharya. Improving common-mode rejection using the right-leg drive amplifier, 2011.
- [BB10] BURR-BROWN. Datasheet: Precision, low power instrumentation amplifier, 2010.
- [BCF<sup>+</sup>05] Terry D. Blumenthal, A Bruce N. Cuthbert, B Diane L. Filion, Steven Hackley, D Ottmar V. Lipp, and Anton Van Boxtel F. Committee report: Guidelines for human startle eyeblink electromyographic studies. *Psychophysiology*, 42:1–15, 2005.
- [BJ85] de Luca CJ. Basmajian JV. *Muscles Alive - The Functions Revealed by Electromyography*. Williams and Wilkins Company, Baltimore, 1985.
- [Bro07] Graham Brooker. *Detection of Signals in Noise*. The University of Sydney, 2007.
- [CIA05] Enrico Costanza, Samuel A. Inverso, and Rebecca Allen. Toward subtle intimate interfaces for mobile devices using an emg controller. In *In CHI 05: Proceedings of the SIGCHI conference on Human factors in computing systems (New)*, pages 481–489. ACM Press, 2005.
- [CIAM07] Enrico Costanza, Samuel A. Inverso, Rebecca Allen, and Pattie Maes. Intimate interfaces in action: assessing the usability and subtlety of emg-based motionless gestures. In *CHI 07*, pages 819–828, 2007.
- [CJDLR10] Mikhail Kuznetsov Carlo J. De Luca, L. Donald Gilmore and Serge H. Roy. Filtering the surface emg signal: Movement artifact and baseline noise contamination. *Journal of Biomechanics (05 March 2010)*, 2010.
- [Dis11] Yosemite Community College District. Physiology 101 - chapter 12 - muscle physiology, 2011.
- [DL97] Carlo J. De Luca. The use of surface electromyography in biomechanics. *Journal of Applied Biomechanics*, 13(2):135–163, 1997.
- [Fri09] A.J. Fridlund. Contour-following integrator for dynamic tracking of electromyographic data. *Psychophysiology*, 1979/09.
- [GD] Atau Tanaka Gilles Dubost. A wireless, network-based biosensor interface for music.
- [Hee98] David Heeger. Signal detection theory, 1998.
- [JER] M.D. John E. Robinton. Surface EMG vs. Needle EMG.
- [Koc07] Volker Maximillian Koch. A factor graph approach to model-based signal separation, 2007.
- [Kon05] Peter Konrad. *EMG-Fibel: Eine praxisorientierte Einführung in die kinesiologische Elektromyographie*. Noraxon INC. USA., 2005.
- [Luc02] Carlo J. De Luca. Surface electromyography - detection and recording, 2002.

- [MC04] N.A. Macmillan and C.D. Creelman. *Detection Theory: A User's Guide*. Taylor & Francis, 2004.
- [NKV<sup>+</sup>] Ganesh R Naik, Dinesh Kant, Kumar Vijay, Pal Singh, and Marimuthu Palaniswami. Hand gestures for hci using ica of emg.
- [PFK97] Foster Provost, Tom Fawcett, and Ron Kohavi. The case against accuracy estimation for comparing induction algorithms. In *In Proceedings of the Fifteenth International Conference on Machine Learning*, pages 445–453. Morgan Kaufmann, 1997.
- [Pro85] J. Proakis. Probability, random variables and stochastic processes. *Acoustics, Speech and Signal Processing, IEEE Transactions on*, 33(6):1637–1637, 1985.
- [RBK90] Hugh S. Lusted R. Benjamin Knapp. Computer music journal - vol. 14, no. 1 - new performance interfaces 1, 1990.
- [RHMY06] M.B.I. Reaz, M.S. Hussain, and F. Mohd-Yasin. Techniques of emg signal analysis - detection, processing, classification and applications, 2006.
- [Tan12] David Tanner. *Probability and the Normal Distribution*. SAGE Publications, Inc., 0 edition, 2012.
- [TKA02] Atau Tanaka, R. Benjamin Knapp, and Rue Amyot. Multimodal interaction in music using the electromyogram and relative position sensing, 2002.
- [TSSB08] Dan Morris T. Scott Saponas, Desney S. Tan and Ravin Balakrishnan. Demonstrating the feasibility of using forearm electromyography for muscle-computer interfaces, 2008.
- [vB08] Anton van Boxtel. Facial emg as a tool for inferring affective states, 2008.
- [Wei06] Martin Weitz. Messung und analyse myoelektrischer signale, 2006.
- [Win99] Uwe Windhorst. *Modern Techniques in Neuroscience Research*. Springer, 1999.
- [XA04] Lanyi X and Adler A. An improved method for muscle activation detection during gait. *Canadian Conference of Electrical and Computer Engineering*, 2004.

## A Additional user study recordings

In addition to tests 1, 2a and 2b another test was completed by the subjects. In this test 3 stimuli tones of a duration of 1 second are played randomly distributed in the range of C3 to C4. In the pause of 2 seconds between the stimuli tones the subject should press the elastic ball with the force corresponding to the heard frequency. As it is very difficult for humans to recognise tone pitch this test was not used in the evaluation. An improvement of test 3 would be to use pitch sweeps as stimuli starting at C3 and rising to the desired tone pitch. Therefore it is more likely that the subject is recognising the correct level.

## B Discrete amplifier test setup

The instrumentation amplifier was discretely built on a development board using three TI082 operational amplifiers by Texas Instruments. The amplified output  $V_{out}$  of the instrumentation amplifier (figure 3.4) was screened and stored on a digital oscilloscope. The screen shot of a short contraction of musculus biceps femoris is shown in figure B.1. Due to the basic circuit design and the lack of filtering and protection by enclosure a quite high unwanted 50Hz hum occurred.

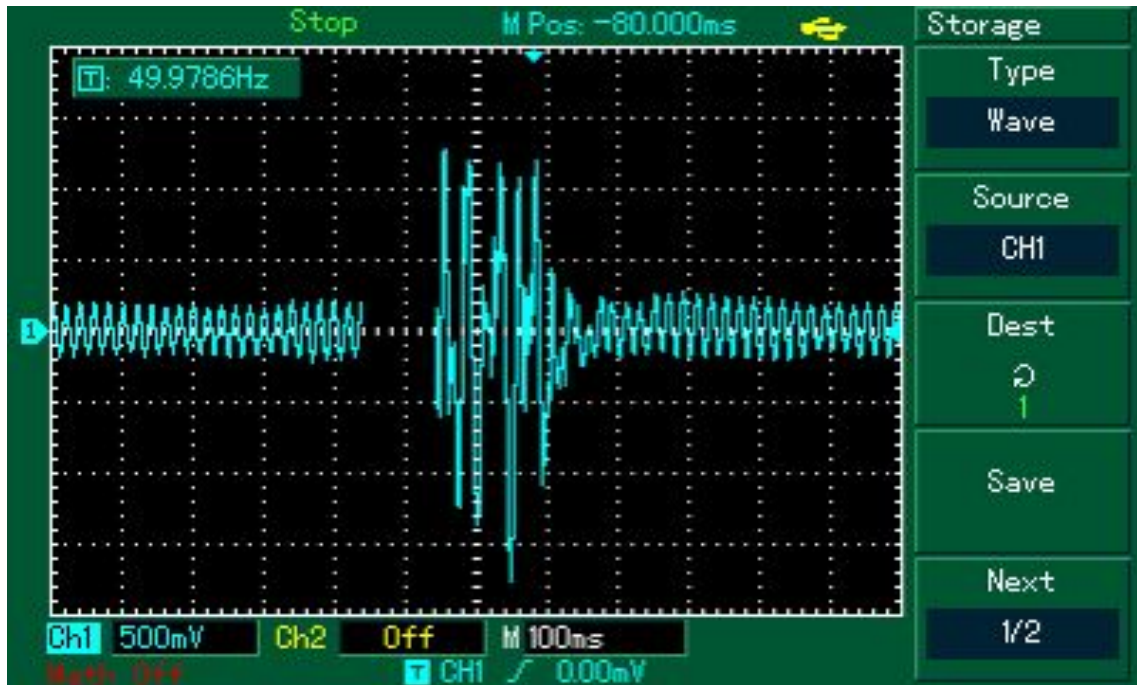


Figure B.1: Recorded waveform of a short contraction of musculus biceps femoris processed with the discrete design, analysed with a digital oscilloscope

## C Printed circuit board layout

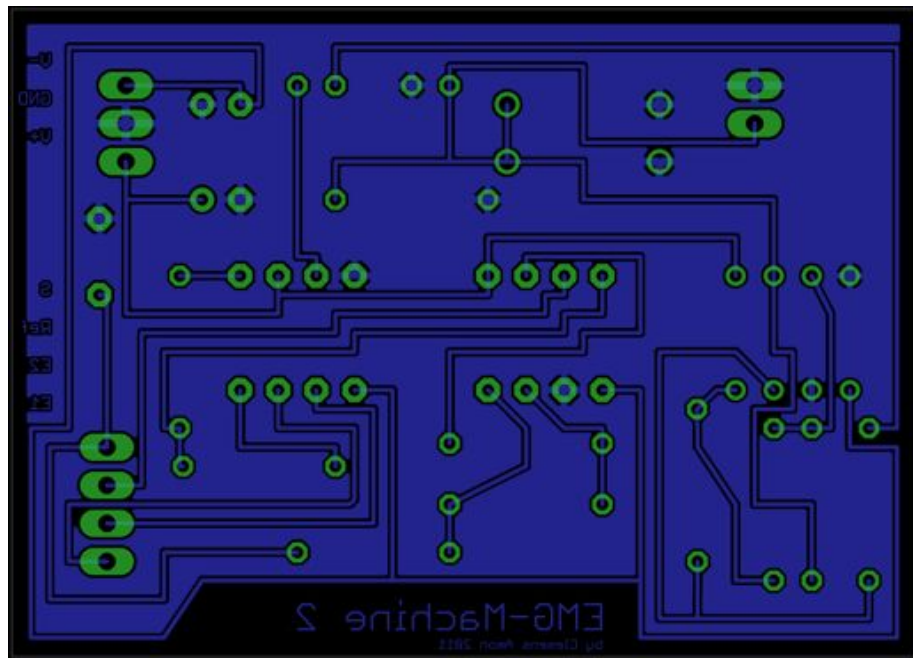


Figure C.1: Printed circuit board layout of "EMG Machine"

### C.1 List of Parts

Table C.1: List of parts required to build 'EMG machine'

Part Description	Quantity
EMG machine 2.0 PCB (figure C.1)	1 Pc
Instrumentation Amp. INA 118P	1 Pc
Wideband Feedback Op. Amp OPA2650P	1 Pc
J-FET Input Op. Amp. TL082P	1 Pc
Resistor 220Ω	2 Pcs
Resistor 1.5 k	1 Pc
Resistor 2.2 kΩ	1 Pc
Resistor 10 kΩ	2 Pcs
Resistor 147 kΩ	1 Pc
Resistor 220 kΩ	3 Pcs
Capacitor 1 μF	2 Pcs
Capacitor 10 nF, 100 pF	1 Pc
Capacitor 100 pF	1 Pc
Diode 1N4004	2 Pcs
PCB Connector	3 Pcs
Metal Housing	1 Pc
Battery 9V	2 Pcs
DC Jack	1 Pc
Audio Plug and Jack mono	1 Pc
Audio Euro Plug and Jack mono	1 Pc
On/Off Switch	1 Pc
Shielded Loudspeaker Cable	8 m
BetterWitts Electrodes	3 Pcs
VELCRO Strap	50 cm
Self Sticking Felt	45 cm <sup>2</sup>
Snap Fastners	3 Pcs